

A genuine test for hyperuniformity

Michael A. Klatt*, Günter Last† and Norbert Henze‡

March 23, 2026

Abstract

We introduce a rigorous and sensitive significance test for hyperuniformity that yields reliable results even from a single sample. Our approach is based on a detailed analysis of the empirical Fourier transform of a stationary point process in \mathbb{R}^d . For large system sizes, we derive the asymptotic covariances and establish a multivariate central limit theorem (CLT) for these empirical Fourier transforms. Their absolute square value, the scattering intensity, is then used as the standard estimator of the structure factor. The above CLT holds for a preferably large class of point processes, and whenever this is the case, the scattering intensity satisfies a multivariate limit theorem as well. Hence, we can use the likelihood ratio principle to test for hyperuniformity. Remarkably, the asymptotic distribution of the resulting test statistic is universal under the null hypothesis of hyperuniformity. We obtain its explicit form from simulations with very high accuracy. The novel test precisely keeps a nominal significance level for hyperuniform models, and it rejects non-hyperuniform examples with high power even in borderline cases. Moreover, it does so given only a single sample with a practically relevant system size.

Keywords: point process, hyperuniformity, structure factor, scattering intensity, central limit theorem, likelihood ratio test

2020 Mathematics Subject Classification: 62H11; 60G55

1 Introduction

Disordered *hyperuniform* point patterns exhibit an anomalous suppression of density fluctuations on large scales [59]. They can be both isotropic like a liquid and homogeneous like a crystal, representing a new state of matter. As a result, they have attracted significant and rapidly growing interest across various disciplines, including physics [61, 19, 59, 48, 41, 63, 54, 58, 20, 2], biology [35, 33], materials science [13, 65, 23],

*michael.klatt@dlr.de; German Aerospace Center (DLR), Institute for AI Safety and Security, Wilhelm-Runge-Str. 10, 89081 Ulm, Germany; German Aerospace Center (DLR), Institute of Frontier Materials on Earth and in Space, Functional, Granular, and Composite Materials, 51170 Cologne, Germany; Department of Physics, LMU München, Schellingstr. 4, 80799 Munich, Germany.

†guenter.last@kit.edu; Karlsruhe Institute of Technology, Institute for Stochastics, 76131 Karlsruhe, Germany.

‡norbert.henze@kit.edu; Karlsruhe Institute of Technology, Institute for Stochastics, 76131 Karlsruhe, Germany.

and probability theory [21, 22, 40, 12, 44, 7, 16, 45, 42, 34], among others. However, despite this widespread interest, a rigorous statistical test to reliably assess the hypothesis of hyperuniformity for a given point pattern has been lacking. This absence poses a risk of ambiguous findings.

Hyperuniformity of a stationary point process is a second-order property and can be defined in either real or Fourier space. In real space, a point process is said to be hyperuniform if, in the limit of large window sizes, the variance of the number of points within a window grows more slowly than the volume of the window. Alternatively, in Fourier space, hyperuniformity is characterized by the vanishing of the so-called *structure factor* at small wave vectors (see [25] and (2.9)). The structure factor is essentially the Fourier transform of the reduced *pair correlation function*, which plays a central role in the theory of point processes [14, 46].

These definitions have led to various ad hoc tests of hyperuniformity based on heuristic principles, which have been widely used in applied research. A straightforward approach estimates the variance of the number of points as a function of the window size [17, 54]. However, this *real space method* requires heuristic rules that avoid a significant overlap between sampling windows [43, 60]. While a rigorous test of hyperuniformity could be designed using independent samples for each observation window, such an approach would require millions of samples [60], making it impractical for real-world applications.

An alternative common approach involves extrapolating the structure factor in the limit of small wave vectors [17, 1, 41]. Typically, this is done via a least-squares fit, which does not enforce the non-negativity constraint of the structure factor, preventing it from serving as a rigorous significance test. This drawback is avoided in a recent work [26] that provides a detailed comparison of different estimators of the structure factor and essentially restricts an empirical test to the smallest accessible wavenumber. However, similar to real space sampling, this approach also requires an independent sample for each data point and does not extrapolate the structure factor to the origin.

In this paper, we address the limitations of previous ad hoc methods by leveraging detailed distributional properties of the empirical Fourier transform. Specifically, we focus on point processes whose estimated structure factor follows a multivariate limit theorem. We hypothesize that this limit theorem holds for a broad class of point processes, an assumption supported by Theorem 4.1 and by [6, Theorem 1]. Additionally, extensive simulations across various point processes further reinforce our hypothesis. By working in an asymptotic setting, we introduce a rigorous *likelihood ratio test* that effectively distinguishes hyperuniform from non-hyperuniform samples for practically relevant models and parameter choices. Our approach relies on asymptotic approximations, which naturally align with the study of a long-range property such as hyperuniformity. Notably, high-precision simulations confirm that these approximations remain accurate even for a moderate system sizes of around 1 000 points per sample. Here, “system size” refers to the mean number of points per sample. Since we work with a fixed number density (intensity), it can also equivalently refer to the linear dimension of the observation window, such as the side length of a cube.

To illustrate the difficulty of distinguishing a hyperuniform point pattern from a non-hyperuniform one by eye, Figure 1 provides an instructive example. The left panel shows a realization of a (non-hyperuniform) Matérn III process near saturation [14]. Although this process exhibits a high degree of local order, it possesses Poisson-like long-range density

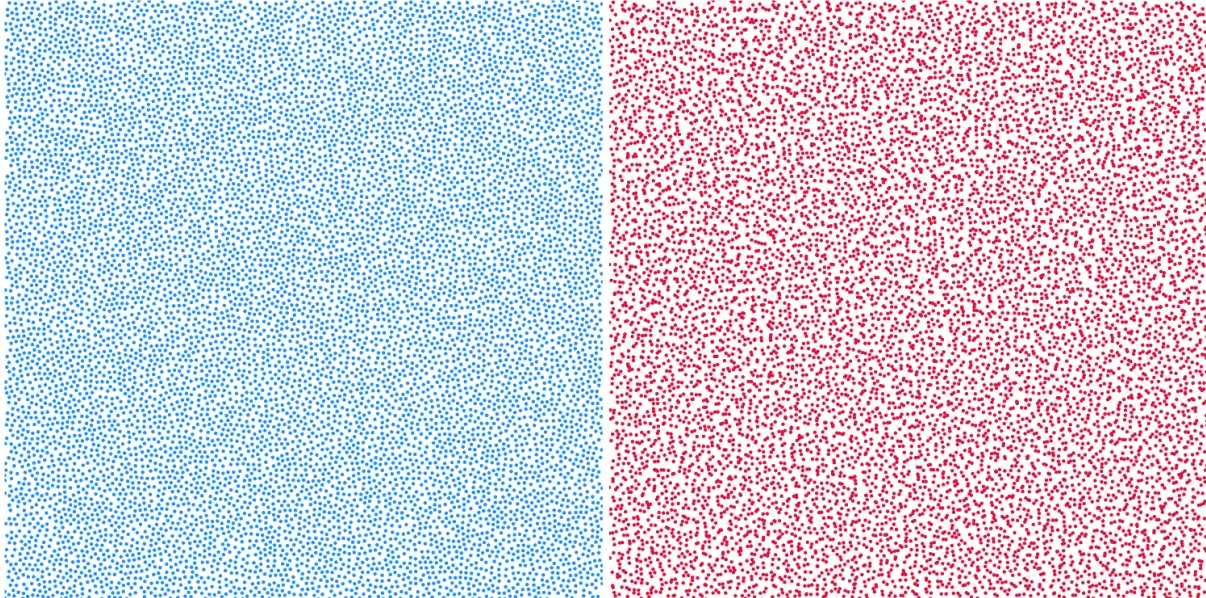


Figure 1: Realizations of a non-hyperuniform (left) and a hyperuniform (right) point process, both with about 10000 points.

fluctuations, which are fundamentally incompatible with hyperuniformity. In contrast, the right panel presents a hyperuniform process. This sample was generated by first simulating a stealthy hyperuniform point pattern [59] and then independently perturbing each point according to a Gaussian distribution. Both processes were simulated on the flat torus. The subtle difference in long-range order between these two samples is clearly detected by our novel test statistic. For the non-hyperuniform sample, the value of the test statistic exceeds 300, far surpassing the critical value of 2.39, which corresponds to a nominal significance level of 5%. In contrast, for the hyperuniform sample, the test statistic attains the value 0.04, demonstrating the remarkable sensitivity of the novel test for assessing hyperuniformity.

We exploit three asymptotic approximations in our test procedure. These approximations are expected to hold simultaneously in the limit of large system sizes; indeed, our simulations indicate rapid convergence even for samples containing only a few hundred points. The three approximations are as follows. First, the previously mentioned multivariate limit theorem. Second, a putative limit theorem for our test statistics, obtained from extensive simulations. Third, a parametric expansion of the structure factor around the origin, which we use to extrapolate its behavior. Specifically, in the third approximation, we assume that the structure factor S satisfies

$$S(k) = s + t\|k\|^\alpha + o(\|k\|^\alpha), \quad \text{as } k \rightarrow 0, \quad (1.1)$$

for some fixed $\alpha > 0$ and parameters $s \geq 0$ and $t \in \mathbb{R}$, at least for wave vectors $k \in \mathbb{R}^d$ in a neighborhood of the origin. In this setting, the hyperuniform case is characterized by $s = 0$. The approximation thus encompasses, in principle, all three classes of hyperuniformity as defined, e.g., in [59]: class I with $\alpha > 1$, class II with $\alpha = 1$, and class III with $0 < \alpha < 1$. The third class corresponds to the least uniform point patterns for which hyperuniformity is most difficult to detect. If there exists an isotropic pair correlation

function g_2 satisfying

$$\int \|x\|^2 |g_2(x) - 1| dx < \infty, \quad (1.2)$$

then assumption (1.1) holds with $\alpha = 2$, which can therefore be considered as the most common case. If $|g_2(x) - 1| \sim \|x\|^{-d-\alpha}$ as $\|x\| \rightarrow \infty$, for $\alpha \in (0, 2)$, then (1.1) holds as well. In the recent preprint [51], the authors assume $s = 0$ and propose methods for estimating the exponent α . In contrast, we fix α (typically $\alpha = 2$) and focus on testing the hyperuniformity hypothesis $s = 0$.

In the following, we summarize our results and relate them to the relevant literature. Section 2 introduces key concepts from the theory of stationary point processes and formally defines hyperuniformity. Following the classical reference [10] (see also the recent survey [26]), Section 3 presents the empirical Fourier transform of a point process, defined using a general taper function. Proposition 3.4 establishes the asymptotic covariance structure of this transform. While the special case $d = 1$ has been implicitly addressed in [10], a rigorous result for general dimensions has, to our knowledge, not been previously established. A related paper is [29], where the authors examine the bias and variance of kernel estimators of the asymptotic variance. In Section 4, we extend a result of [10] to general dimensions by proving a multivariate central limit theorem (CLT) for the empirical Fourier transform (Theorem 4.1). As in [10], we rely on an assumption regarding the reduced factorial cumulant measures. Our proof does also benefit from the classical work of [30], which employs a similar hypothesis to establish a related CLT; see also [28] for a more recent contribution to the asymptotic normality of kernel estimators of correlation functions. We illustrate our findings using Poisson cluster and α -determinantal processes.

In the following, we use the *empirical scattering intensity* (2.12) as a well-established estimator of the structure factor; see [59]. Section 5 explores its multivariate asymptotic behavior for different wave vectors and for large system sizes. We will see that the resulting limit distribution consists of exponential random variables, which are independent across different wave vectors (Proposition 5.2). This crucial result requires the underlying point process to satisfy the multivariate central limit theorem (4.9). Theoretically, this assumption is supported by Theorem 4.1 and [6, Theorem 1]; see Remark 5.1. To validate these theoretical findings, we have simulated six different models, including two hyperuniform ones, across the first three dimensions. In each case, the theoretically predicted behavior is observed over up to six orders of magnitude, even for small system sizes of about 1 000 points. These simulations indicate a fast rate of convergence, ensuring that the asymptotic distribution is attained with high accuracy at practically relevant system sizes.

In Section 6, we shift the focus from point processes to the asymptotic setting established in Proposition 5.2. By employing the parametrization (1.1) of the structure factor, we obtain a statistical model with only two parameters, denoted as s and t . This additional approximation and simplification can be justified by taking sufficiently large system sizes. Within this framework, hyperuniformity is characterized by the equation $s = 0$, defining the null hypothesis H_0 . To test this hypothesis, we introduce *maximum likelihood estimators* \hat{t}_0 of t under the null hypothesis and (\hat{s}, \hat{t}_1) of (s, t) under the full model, respectively. Under H_0 , the estimator \hat{t}_0 of t is unbiased and consistent when applied to random data, following an exact gamma distribution for finite system sizes.

Under the full model we observe that, asymptotically, the distribution of \widehat{s} equals a mixture of the Dirac distribution at 0 and a gamma distribution, while \widehat{t}_1 follows a gamma distribution. In particular, the distribution of \widehat{s} has an atom at 0. These findings are based on numerical solutions of the likelihood equations and extensive simulations.

In Section 7, we introduce our likelihood ratio test. Within the asymptotic and parametric setting of Section 6, we analyze the ratio of the maximum likelihood of the data under the null hypothesis to the corresponding maximum likelihood over the full parameter space. The resulting test statistic is twice the negative logarithm of this ratio. Analytically, the asymptotic null distribution of this test statistic appears to be out of reach. However, through extensive simulations, we have determined this distribution with high accuracy. Our empirical results indicate that this limit null distribution consists of a mixture of an atomic component at 0 (inherited from \widehat{s}) and a gamma distribution. Notably, this distribution already applies for moderate system sizes. Furthermore, we rigorously demonstrate that this limit distribution does not depend on the specific value of the parameter t . This result enables a significance test for hyperuniformity, which can be conveniently applied to spatial point patterns encountered in real-world applications.

In Section 8, we apply the novel test to independent thinnings of the matching process from [40]; see also Example (v) in Section 5. Introducing a thinning parameter provides a convenient way to tune the parameter s . The hyperuniform case $s = 0$ corresponds to the limit case of no thinning. Our findings confirm that the asymptotic distribution of the test statistic applies extremely well to this point process. Remarkably, the test performs reliably even for a single sample with a moderately large system size.

We apply our test with a nominal significance level of 0.05 for different values of the parameter s . When $s = 0$, the test accurately maintains the nominal level. Even for $s = 10^{-3}$ and a system size of $L = 150$ in two dimensions (i.e., for about 150^2 points), the test rejects hyperuniformity in almost all cases. Furthermore for $s = 10^{-4}$, which is an order of magnitude smaller than typical non-hyperuniform models (see [59, 41]), the rejection rate increases dramatically as the systems size grows; see Table 1 for more details.

We conclude the paper with a summary of the test procedure and remarks on the fundamental principles underlying the novel test. We then outline several interesting open problems for future research directions. For the sake of readability, some proofs have been moved to an appendix.

2 Preliminaries

We begin by introducing some point process terminology, primarily drawn from Chapters 8 and 9 of [46]. Our setting is \mathbb{R}^d for $d \geq 1$, equipped with the Borel σ -field \mathcal{B}^d and Lebesgue measure λ_d . Let \mathcal{B}_b^d denote the collection of bounded elements of \mathcal{B}^d , and let \mathbf{N} represent the system of locally finite subsets of \mathbb{R}^d . For $\mu \in \mathbf{N}$ and $B \subset \mathbb{R}^d$ we denote by $\mu(B)$ the cardinality of $\mu \cap B$. By definition, $\mu(B) \in \mathbb{N}_0$ for each $B \in \mathcal{B}_b^d$. We define \mathcal{N} as the smallest σ -field on \mathbf{N} that makes the mappings $\mu \mapsto \mu(B)$ measurable for each $B \in \mathcal{B}^d$.

A (simple) *point process* is a random element η of $(\mathbf{N}, \mathcal{N})$, defined on some fixed probability space $(\Omega, \mathcal{F}, \mathbb{P})$ with associated expectation operator \mathbb{E} . The process is said

to be *stationary* if the distribution of $\eta + x := \{y + x : y \in \eta\}$ does not depend on $x \in \mathbb{R}^d$. In this case, $\gamma := \mathbb{E}\eta([0, 1]^d)$ is called the *intensity* (or, in physics terminology, the *number density*) of η . By Campbell's formula,

$$\mathbb{E} \sum_{x \in \eta} f(x) = \gamma \int f(x) dx \quad (2.1)$$

for each measurable function $f: \mathbb{R}^d \rightarrow [0, \infty)$. Here and in what follows, each unspecified integral is over the full domain.

We consider a stationary point process η with positive and finite intensity γ . Additionally, we assume that η is *locally square integrable*, meaning that $\mathbb{E}\eta(B)^2 < \infty$ for each $B \in \mathcal{B}_b^d$. The *second factorial moment measure* α_2 of η is defined by

$$\alpha_2(\cdot) := \mathbb{E} \sum_{x, y \in \eta} \mathbf{1}\{x \in [0, 1]^d, y - x \in \cdot\},$$

where $\mathbf{1}\{\cdot\}$ stands for the indicator function. It is often more convenient to work with the *reduced second factorial moment measure* α_2^\dagger of η , defined by

$$\alpha_2^\dagger(\cdot) := \mathbb{E} \sum_{x, y \in \eta}^{\neq} \mathbf{1}\{x \in [0, 1]^d, y - x \in \cdot\}.$$

Here, the superscript \neq indicates that the summation is taken over distinct pairs. From the definition and (2.1), it follows that $\alpha_2 = \alpha_2^\dagger + \gamma\delta_0$, where δ_0 is the *Dirac measure* at $0 \in \mathbb{R}^d$. Note that α_2^\dagger is a locally finite measure on \mathbb{R}^d , which is invariant under reflections at the origin. Moreover, it satisfies the equation

$$\mathbb{E} \sum_{x, y \in \eta}^{\neq} \mathbf{1}\{(x, y) \in \cdot\} = \iint \mathbf{1}\{(x, x + y) \in \cdot\} \alpha_2^\dagger(dy) dx. \quad (2.2)$$

In many cases, the measure α_2^\dagger admits a density with respect to the Lebesgue measure, which gives

$$\alpha_2^\dagger(dy) = \gamma^2 g_2(y) dy,$$

where $g_2: \mathbb{R}^d \rightarrow [0, \infty)$ is the so-called *pair correlation function* of η . This function is measurable and locally integrable, and it can be assumed to satisfy the symmetry property $g_2(x) = g_2(-x)$ for each $x \in \mathbb{R}^d$. For any $B \in \mathcal{B}^d$, it follows from (2.2) that

$$\mathbb{E}\eta(B)^2 = \gamma\lambda_d(B) + \iint \mathbf{1}\{x \in B, x + y \in B\} dx \alpha_2^\dagger(dy);$$

see [46, (4.25) and (8.8)]. If B is bounded, then the variance of $\eta(B)$ is given by

$$\text{Var} \eta(B) = \gamma\lambda_d(B) + \int \lambda_d(B \cap (B + y)) \alpha_2^\dagger(dy) - \gamma^2\lambda_d(B)^2.$$

Since $\int \lambda_d(B \cap (B + y)) dy = \lambda_d(B)^2$, an alternative representation of the variance is

$$\text{Var} \eta(B) = \gamma\lambda_d(B) + \int \lambda_d(B \cap (B + y)) \beta_2^\dagger(dy), \quad (2.3)$$

where the *signed measure* $\beta_2^!$ is defined as

$$\beta_2^! := \alpha_2^! - \gamma^2 \lambda_d. \quad (2.4)$$

The measure $\beta_2 := \beta_2^! + \gamma \delta_0 = \alpha_2 - \gamma^2 \lambda_d$ is the *covariance measure* of η ; see [9, Chapter 9]. In fact, $\beta_2^!$ is the second reduced factorial cumulant measure of η , which is a special case of a locally finite measure $\beta_m^!$, defined in (4.7) for each integer $m \geq 2$. The covariance measure is only defined on the system of bounded Borel sets of \mathbb{R}^d . The restriction $\beta_2^!(B \cap \cdot)$ of $\beta_2^!$ onto a bounded Borel subset B of \mathbb{R}^d is a finite signed measure, which hence can be written as the difference of two orthogonal finite measures. This allows us to define the *total variation measure* $|\beta_2^!|$, first on B , and then, by consistency, on each Borel set. The result is a locally finite measure on \mathbb{R}^d . If the point process η has a pair correlation function g_2 , then

$$\beta_2^!(dx) = \gamma^2(g_2(x) - 1) dx$$

and

$$|\beta_2^!|(dx) = \gamma^2|g_2(x) - 1| dx. \quad (2.5)$$

In Sections 3 and 4, we assume that

$$|\beta_2^!|(\mathbb{R}^d) < \infty. \quad (2.6)$$

Clearly, this condition is equivalent to $|\beta_2|(\mathbb{R}^d) < \infty$.

Let $W \subset \mathbb{R}^d$ be a convex compact set with a non-empty interior. For each $y \in \mathbb{R}^d$, we have $\lim_{r \rightarrow \infty} \lambda_d(rW)^{-1} \lambda_d(rW \cap (rW + y)) = 1$. If condition (2.6) holds, it follows from (2.3) and the dominated convergence theorem that

$$\lim_{r \rightarrow \infty} \frac{\text{Var } \eta(rW)}{\lambda_d(rW)} = \gamma + \beta_2^!(\mathbb{R}^d). \quad (2.7)$$

The point process η is said to be *hyperuniform* with respect to W if

$$\lim_{r \rightarrow \infty} \frac{\text{Var } \eta(rW)}{\lambda_d(rW)} = 0.$$

If this convergence holds with W chosen as the unit ball $B_1 := \{x \in \mathbb{R}^d : \|x\| \leq 1\}$, where $\|\cdot\|$ denotes the Euclidean norm, we simply say that η is hyperuniform [61, 59]. If condition (2.6) holds, then (2.7) shows that hyperuniformity is equivalent to

$$\beta_2^!(\mathbb{R}^d) = -\gamma. \quad (2.8)$$

For the remainder of this section, we assume that condition (2.6) holds. Let i denote the imaginary unit, and let $\langle \cdot, \cdot \rangle$ represent the inner product on $\mathbb{R}^d \times \mathbb{R}^d$. The *structure factor* S of η is the function on \mathbb{R}^d defined by

$$S(k) := 1 + \frac{1}{\gamma} \int e^{-i\langle k, x \rangle} \beta_2^!(dx), \quad k \in \mathbb{R}^d. \quad (2.9)$$

This definition is justified by assumption (2.6). If η has a pair correlation function, then the structure factor is given by

$$S(k) = 1 + \gamma \int e^{-i\langle k, x \rangle} (g_2(x) - 1) dx, \quad k \in \mathbb{R}^d.$$

Thus, $\gamma^{-1}(S - 1)$ is the Fourier transform of $g_2 - 1$. In the general case, $\gamma^{-1}(S - 1)$ is the Fourier transform of the covariance measure. Since $\beta_2^!$ is reflection-invariant, the function S is real-valued, and we have $S(k) = S(-k)$ for each $k \in \mathbb{R}^d$. Finally, hyperuniformity is equivalent to

$$S(0) = 0.$$

Throughout this paper, the symbol 0 stands for the origin in \mathbb{R}^d for any $d \geq 1$, which includes, in particular, the real number zero. The specific meaning of 0 will always be clear from the context.

In the important special case of a *perturbed lattice*, assumption (2.6) does not hold; see, e.g., [39]. Nevertheless, it is still possible to define the structure factor in such cases, at least in a neighborhood of the origin. To achieve this, we introduce the *Fourier transform* $\hat{\beta}_2$ of β_2 , which is a locally finite measure on \mathbb{R}^d satisfying

$$\int (f \star g)(x) \beta_2(dx) = \frac{1}{(2\pi)^d} \int \hat{f}(k) \hat{g}(-k) \hat{\beta}_2(dk), \quad (2.10)$$

for all bounded measurable functions $f, g: \mathbb{R}^d \rightarrow \mathbb{R}$ with bounded support, where the *tilted convolution* $(f \star g)$ is defined as $(f \star g)(x) := \int f(x)g(x - y) dy$, $y \in \mathbb{R}^d$. This measure is also known as the *Bartlett spectral measure* of η ; see [9, Chapter 9]. If β_2 has finite total variation, then

$$\hat{\beta}_2(dk) = \gamma S(k) dk, \quad (2.11)$$

where $S(k) := \gamma^{-1} \int e^{-i\langle k, x \rangle} \beta_2(dx)$, $k \in \mathbb{R}^d$. We continue to refer to the function S as the structure factor, even if equation (2.11) holds only in a neighborhood of the origin. If η is a (stationary) perturbed lattice based on a *lattice* $\mathbb{L} \subset \mathbb{R}^d$ and the distribution \mathbb{Q} of independent translations, then

$$\hat{\beta}_2(dk) = (1 - |\hat{\mathbb{Q}}|^2(k)) dk + \sum_{l \in \mathbb{L}^* \setminus \{0\}} |\hat{\mathbb{Q}}(k)|^2 \delta_l(dk),$$

where $\hat{\mathbb{Q}}$ is the Fourier transform of \mathbb{Q} , and \mathbb{L}^* denotes the *dual lattice* of \mathbb{L} . Hence, we may define $S(k) := 1 - |\hat{\mathbb{Q}}(k)|^2$, except at points in $\mathbb{L}^* \setminus \{0\}$. If $\int \|x\|^2 \mathbb{Q}(dk) < \infty$ and \mathbb{Q} is isotropic (i.e., invariant under rotations), then (1.1) holds with $\alpha = 2$. We refer to [18, 39, 59, 7] for more details on perturbed lattices and their Fourier transforms.

Assuming that (1.1) holds, we test the hypothesis $S(0) = 0$ (i.e., hyperuniformity) using the empirical *scattering intensity*

$$\mathcal{S}_r(k) := \frac{1}{\eta(W_r)} \left| \sum_{x \in \eta \cap W_r} e^{-i\langle k, x \rangle} - \mathbf{1}\{k = 0\} \gamma r^d \right|^2, \quad k \in \mathbb{R}^d, \quad (2.12)$$

where $1/0 := 0$, and W_r is a cube centered at 0 with side length $r > 0$.

3 Asymptotic covariance structure

In this section, we assume that

$$\int (1 + \|x\|^p) |\beta_2^!|(dx) < \infty, \quad (3.1)$$

for some $p > 0$, which strengthens condition (2.6). If, for instance, $|g_2(x) - 1| \sim \|x\|^{-d-\alpha}$ as $\|x\| \rightarrow \infty$, for some $\alpha \in (0, 2)$, then (1.1) holds and we can choose $p < \alpha$. Since $\beta_2^!$ is locally finite, we can assume $p \leq 1$ without loss of generality.

We fix a bounded and measurable function $h: \mathbb{R}^d \rightarrow [0, \infty)$ satisfying

$$M_1(h) < \infty, \quad (3.2)$$

where

$$M_j(h) := \int h(x)^j dx, \quad j = 1, 2.$$

Since h is bounded, it follows from (3.2) that $M_2(h) < \infty$. We also assume the existence of constants $a, b > 0$ such that

$$\mathbf{1}\{\|y\| \leq b\} \int |h(x+y) - h(x)| dx \leq a\|y\|^p, \quad (3.3)$$

where $p > 0$ is as in assumption (3.1). Note that if (3.3) holds for $p = 1$ (or $p > 1$) then it holds for each $p \leq 1$. This only requires replacing the constant a by ab^{1-p} . Note also that

$$\int |h(x+y) - h(x)| dx \leq 2M_1(h), \quad y \in \mathbb{R}^d.$$

The class of measurable bounded functions $h: \mathbb{R}^d \rightarrow [0, \infty)$ that satisfy conditions (3.2) and (3.3) is denoted by \mathcal{H}_p .

Throughout this article we take $h \in \mathcal{H}_p$ for some (suitable) $p > 0$. Since $M_2(h) < \infty$ we have by the Riemann–Lebesgue lemma

$$\lim_{\|k\| \rightarrow \infty} \int h(x)^2 e^{i\langle k, x \rangle} dx = 0. \quad (3.4)$$

For $r > 0$, we define the rescaled function $h_r(x) := h(x/r)$. Observing that $\int h_r(x)^j dx = M_j(h)r^d$ for $j \in \{1, 2\}$, we note that

$$\frac{1}{r^d} \int h_r(x)^2 e^{i\langle k, x \rangle} dx = \int h(x)^2 e^{i\langle rk, x \rangle} dx, \quad k \in \mathbb{R}^d. \quad (3.5)$$

Later, we consider functions $r \mapsto k_r$ from $(0, \infty)$ to \mathbb{R}^d , abbreviated as (k_r) , satisfying $k_\infty := \lim_{r \rightarrow \infty} k_r \neq 0$ and

$$\lim_{r \rightarrow \infty} \frac{1}{r^{d/2}} \int h_r(x) e^{i\langle k_r, x \rangle} dx = \lim_{r \rightarrow \infty} \frac{1}{r^{d/2}} \int h_r(x) e^{-i\langle k_r, x \rangle} dx = 0. \quad (3.6)$$

The space of all such functions is denoted by \mathbf{F} . We also frequently consider the extended space $\mathbf{F} \cup \{\mathbf{0}\}$, where $\mathbf{0}$ is the zero function.

Example 3.1. Let $B_r \subset \mathbb{R}^d$ denote the closed ball with radius r , centered at the origin, and let $\kappa_d = \pi^{d/2}/\Gamma(1 + d/2)$ denote the volume of B_1 . Let $r_d > 0$ satisfy $\kappa_d r_d^d = 1$, so that B_{r_d} has volume 1. Let h be the indicator function of B_{r_d} . Then $M_1(h) = M_2(h) = 1$, and the rescaled function h_r is the indicator function of a ball with radius rr_d . To verify condition (3.6), we use a classical result concerning the Fourier transform of the indicator function of a ball; see, e.g., [24, Section B.5]. Specifically, for each $r > 0$,

$$\int_{B_r} e^{i\langle k, x \rangle} dx = \left(\frac{2\pi r}{\|k\|} \right)^{d/2} J_{d/2}(\|k\|r), \quad k \in \mathbb{R}^d \setminus \{0\},$$

where $J_a: [0, \infty) \rightarrow \mathbb{R}$ is the *Bessel function of the first kind*, defined for $a > -1/2$ as

$$J_a(t) := \sum_{m=0}^{\infty} \frac{(-1)^m}{m! \Gamma(m + a + 1)} \left(\frac{t}{2} \right)^{2m+a}, \quad t \geq 0.$$

Since $\lim_{t \rightarrow \infty} J_a(t) = 0$ (see [24, Section B.8]), condition (3.6) holds for any function (k_r) with a non-trivial limit.

To verify (3.3), define $a_+ := \max(0, a)$ for $a \in \mathbb{R}$ and fix $y \in \mathbb{R}^d$. If $x \in B_{r_d}$, but $x + y \notin B_{r_d}$, and if $\|y\| \leq r_d$, the triangle inequality implies $r_d - \|y\| \leq \|x\|$. Thus,

$$\begin{aligned} & \int \mathbf{1}\{x \in B_{r_d}, x + y \notin B_{r_d}\} dx \\ & \leq \mathbf{1}\{\|y\| \leq r_d\} \int \mathbf{1}\{x \in B_{r_d} \setminus B_{(r_d - \|y\|)_+}\} dx + \mathbf{1}\{\|y\| > r_d\}. \end{aligned}$$

(Note that this inequality holds trivially if $\|y\| > r_d$.) The first term can be bounded by

$$\begin{aligned} \mathbf{1}\{\|y\| \leq r_d\} (\kappa_d r_d^d - \kappa_d (r_d - \|y\|)^d) & \leq \mathbf{1}\{\|y\| \leq r_d\} \sum_{j=0}^{d-1} c_j r_d^j \|y\|^{d-j} \\ & \leq \mathbf{1}\{\|y\| \leq r_d\} \|y\| \sum_{j=0}^{d-1} c_j r_d^{d-1}, \end{aligned}$$

for some positive constants c_0, \dots, c_{d-1} . Since the same bound applies to

$$\int \mathbf{1}\{x \notin B_{r_d}, x + y \in B_{r_d}\} dx = \int \mathbf{1}\{x - y \notin B_{r_d}, x \in B_{r_d}\} dx,$$

it follows that (3.3) holds for $p = 1$, showing that $h \in \mathcal{H}_p$ for $p \leq 1$.

Example 3.2. Assume that h is the indicator function of the unit cube $W_1 := [-1/2, 1/2]^d$, centered at the origin. Then $M_1(h) = M_2(h) = 1$, and h_r is the indicator function of the cube $W_r := [-r/2, r/2]^d$. A straightforward calculation yields

$$\int_{W_r} e^{i\langle k, x \rangle} dx = \prod_{j=1}^d \frac{2}{k_j} \sin \frac{k_j r}{2}, \quad k = (k_1, \dots, k_d) \in \mathbb{R}^d,$$

where we define $\sin st/s := t$ for $s = 0$. Thus, (3.6) is valid for each function (k_r) that has a limit in the set

$$A_{\square} := \left\{ k \in \mathbb{R}^d : \sum_{i=1}^d \mathbf{1}\{|k_i| > 0\} > \frac{d}{2} \right\}. \quad (3.7)$$

If $d = 2$, then $A_{\square} = \{(k_1, k_2) : k_1 k_2 \neq 0\}$. Furthermore, equation (3.6) also holds if $k_r r \in 2\pi\mathbb{Z}^d$ for each $r > 0$, in which case the integral in (3.6) vanishes. Relation (3.3) can be checked as in Example 3.1.

Example 3.3. Now, assume that $h(x) = (2\pi)^{-d/2} e^{-\|x\|^2/2}$ is the density of the standard normal distribution. Then

$$\int h(x) e^{i\langle k, x \rangle} dx = e^{-\|k\|^2/2}, \quad k \in \mathbb{R}^d, \quad (3.8)$$

$$\int h(x)^2 e^{i\langle k, x \rangle} dx = \pi^{-d/2} e^{-\|k\|^2}, \quad k \in \mathbb{R}^d. \quad (3.9)$$

Hence (3.6) is valid for any (k_r) with a non-trivial limit. We now assert that $h \in \mathcal{H}_1$, meaning that (3.3) holds for $p = 1$. To verify this, we apply the mean value theorem. For $x, y \in \mathbb{R}^d$, we obtain $h(x+y) - h(x) = \langle h'(x + \vartheta), y \rangle$, where h' is the gradient of h and $\vartheta \in [0, 1]$ depends on x and y . Consequently,

$$|h(x+y) - h(x)| = c e^{-\|x+\vartheta y\|^2/2} |\langle x + \vartheta y, y \rangle|,$$

where $c := (2\pi)^{-d/2}$. It follows that

$$\int |h(x+y) - h(x)| dx \leq c \|y\| \int \|x\| e^{-\|x+\vartheta y\|^2/2} dx + c \|y\|^2 \int e^{-\|x+\vartheta y\|^2/2} dx.$$

Now, assume that $\|y\| \leq 1$. It is easy to verify that $\|x + \vartheta y\| \geq \|x\|/2$ whenever $\|x\| \geq 2$. By splitting the domain of integration into $\|x\| < 2$ and $\|x\| \geq 2$, it follows that (3.3) holds for $p = 1$ and $b = 1$. Further details are left to the reader.

Similarly to [10], we define, for each $r > 0$, a random function T_r on \mathbb{R}^d by

$$T_r(k) := \frac{1}{r^{d/2}} \sum_{x \in \eta} h_r(x) e^{-i\langle k, x \rangle} - \mathbf{1}\{k = 0\} M_1(h) \gamma r^{d/2}, \quad k \in \mathbb{R}^d. \quad (3.10)$$

In the language of point process theory, $T_r(k)$ is a linear function of η . Note that $T_r(-k)$ is the complex conjugate $\overline{T_r(k)}$ of $T_r(k)$. In the case of Example 3.2, T_r is closely related to the scattering intensity given in (2.12). In this context, the function h appearing in (3.10) is referred to as a *taper function*; see [10, 56]. In physics, the variables defined in (3.10) are known as *collective coordinates*; see [62]. If $(k_r) \in \mathbf{F} \cup \{\mathbf{0}\}$, then applying Campbell's formula (2.1) along with (3.6) yields

$$\lim_{r \rightarrow \infty} \mathbb{E} T_r(k_r) = 0. \quad (3.11)$$

In fact, if $(k_r) = \mathbf{0}$ then $\mathbb{E} T_r(k_r) = 0$ for each $r > 0$. The following result describes the asymptotic behavior of the covariances of the functionals T_r . The proof is given in the Appendix; see Subsection 11.1.

Proposition 3.4. *Suppose that $(k_r), (\ell_r) \in \mathbf{F} \cup \{\mathbf{0}\}$, and set $k := k_\infty$ and $\ell := \ell_\infty$. If $k \neq \ell$, then*

$$\lim_{r \rightarrow \infty} \mathbb{E} T_r(k_r) \overline{T_r(\ell_r)} = 0. \quad (3.12)$$

Furthermore,

$$\lim_{r \rightarrow \infty} \mathbb{E} |T_r(k_r)|^2 = \gamma M_2(h) S(k). \quad (3.13)$$

Later, we will use the following non-asymptotic result.

Corollary 3.5. *Assume that (2.6) holds. Let $r > 0$ and $k \in \mathbb{R}^d \setminus \{0\}$. Then*

$$\begin{aligned} \mathbb{E} |T_r(k)|^2 &= \gamma M_2(h) S(k) + \frac{1}{r^d} \iint h_r(x) (h_r(x+y) - h_r(x)) e^{i\langle k, y \rangle} dx \beta_2^!(dy) \\ &\quad + \frac{\gamma^2}{r^d} \left| \int h_r(x) e^{-i\langle k, x \rangle} dx \right|^2. \end{aligned} \quad (3.14)$$

Proof. By (11.1), we have

$$\mathbb{E} |T_r(k)|^2 = \gamma M_2(h) + \frac{1}{r^d} \iint h_r(x) h_r(x+y) e^{i\langle k, y \rangle} dx \alpha_2^!(dy).$$

Using (2.4), this can be rewritten as

$$\mathbb{E} |T_r(k)|^2 = \gamma M_2(h) + A_r + B_r,$$

where

$$\begin{aligned} A_r &:= \frac{1}{r^d} \iint h_r(x) h_r(x+y) e^{i\langle k, y \rangle} dx \beta_2^!(dy), \\ B_r &:= \frac{\gamma^2}{r^d} \iint h_r(x) h_r(x+y) e^{-i\langle k, y \rangle} dx dy. \end{aligned}$$

Since $e^{i\langle k, y \rangle} = e^{i\langle k, x \rangle} e^{-i\langle k, x+y \rangle}$, it follows that B_r corresponds to the third term on the right-hand side of (3.14). Moreover, we obtain

$$A_r = M_2(h) \int e^{i\langle k, y \rangle} \beta_2^!(dy) + \frac{1}{r^d} \iint h_r(x) (h_r(x+y) - h_r(x)) e^{i\langle k, y \rangle} dx \beta_2^!(dy),$$

which concludes the proof. \square

Remark 3.6. In general, Proposition 3.4 does not hold for functions $(k_r), (\ell_r)$ that tend to zero in a non-trivial manner. For example, consider $(k_r) = \mathbf{0}$ and $\ell_r = \pi/r$. Then the first term on the right-hand side of (11.2) equals $\gamma \int h(x)^2 e^{i\langle \pi, x \rangle} dx$. Combining this with (11.3), we obtain

$$\lim_{r \rightarrow \infty} \mathbb{E} T_r(0) \overline{T_r(\ell_r)} = (\gamma + \beta_2^!(\mathbb{R}^d)) \int h(x)^2 e^{i\langle \pi, x \rangle} dx,$$

which is not equal to $\gamma M_2(h)$.

For $k \in \mathbb{R}^d$ and $r > 0$, we denote by $T_{r,1}(k)$ the real part and by $T_{r,2}(k)$ the imaginary part of $T_r(k)$. Given $(k_r), (\ell_r) \in \mathbf{F} \cup \{\mathbf{0}\}$, we define

$$\sigma_{m,n}(k, \ell) := \lim_{r \rightarrow \infty} \mathbb{E} T_{r,m}(k_r) T_{r,n}(\ell_r), \quad m, n \in \{1, 2\}, \quad (3.15)$$

where $k := k_\infty$ and $\ell := \ell_\infty$. This definition is justified by Proposition 3.4. We also define the set

$$A_h := \{k_\infty : (k_r) \in \mathbf{F}\} \cup \{\mathbf{0}\}, \quad (3.16)$$

noting that $A_h = -A_h$.

Corollary 3.7. *Let $k, \ell \in A_h$ such that either $k = \ell$ or $k \notin \{\ell, -\ell\}$. Then*

$$\sigma_{m,n}(k, \ell) = \mathbf{1}\{m = n, k = \ell\} \frac{\gamma M_2(h) S(k)}{2}, \quad m, n \in \{1, 2\}. \quad (3.17)$$

Proof. By (3.13),

$$\sigma_{1,1}(k, k) + \sigma_{2,2}(k, k) = \gamma M_2(h) S(k).$$

We also have the trivial identity $\sigma_{1,2}(k, k) = \sigma_{2,1}(k, k)$.

Applying (3.12) with $\ell = -k$ and using the property $T_r(-k) = \overline{T_r(k)}$, we obtain

$$\sigma_{1,1}(k, k) - \sigma_{2,2}(k, k) = \sigma_{1,2}(k, k) + \sigma_{2,1}(k, k) = 0.$$

Thus, (3.17) holds for $k = \ell$. Now, assume that $k \notin \{\ell, -\ell\}$. Applying (3.12) with ℓ and $-\ell$, it follows that $\sigma_{m,n}(k, \ell) = 0$ for all $m, n \in \{1, 2\}$. \square

Remark 3.8. Assume that h is the cubic taper function from Example 3.2. Let $r > 0$ and $k = (k_1, \dots, k_d) \in \mathbb{R}^d \setminus \{0\}$. Assuming (3.1), it follows from Corollary 3.5 and a straightforward computation that

$$\mathbb{E}|T_r(k)|^2 = \gamma S(k) + f_r(k) + \frac{\gamma^2}{r^d} \left| \prod_{j=1}^d \int_{-r/2}^{r/2} e^{-ik_j s} ds \right|^2, \quad (3.18)$$

where

$$f_r(k) := \frac{1}{r^d} \iint h_r(x) (h_r(x+y) - h_r(x)) e^{i\langle k, y \rangle} dx \beta_2^1(dy).$$

From the proof of Proposition 3.4, it follows that

$$\sup_{k \in \mathbb{R}^d \setminus \{0\}} |f_r(k)| \rightarrow 0, \quad \text{as } r \rightarrow \infty.$$

If $k_j = 2\pi n/r$ for some $j \in [d]$ and $n \in \mathbb{N}$, then the last term on the right-hand side of (3.18) vanishes. Let

$$K'_r := \{k \in \mathbb{R}^d : k_j = 2\pi n/r \text{ for some } j \in [d] \text{ and } n \geq 1\}. \quad (3.19)$$

Then

$$\sup_{k \in K'_r} |\gamma^{-1} \mathbb{E}|T_r(k)|^2 - S(k)| \rightarrow 0, \quad \text{as } r \rightarrow \infty.$$

On the other hand, we may choose $k_j \equiv k_j(r) = \pi/r$ for each $j \in [d]$; see also Remark 3.6. Then, for any $\varepsilon > 0$, equation (3.18) implies that

$$\sup_{k \in \mathbb{R}^d \setminus \{0\}, \|k\| \leq \varepsilon} |\gamma^{-1} \mathbb{E}|T_r(k)|^2 - S(k)| \rightarrow \infty, \quad \text{as } r \rightarrow \infty.$$

In our statistical setting we will work with a cubic taper function. For fixed r , we will always choose the wave vectors from the set $K_r \subset K'_r$, which is defined by (6.4) after replacing the system-size label L by r (i.e., $K_r = K'_L$). This choice is commonly adopted in the physics literature [59, 25], see also [26] for a recent mathematical discussion and [49] for a related study in physics, and it is also supported by Corollary 4.2.

4 A central limit theorem

In this section, let η be a stationary point process with intensity γ satisfying

$$\mathbb{E}\eta(B)^m < \infty \tag{4.1}$$

for each bounded Borel set $B \subset \mathbb{R}^d$ and each $m \in \mathbb{N}$. We assume $h \in \mathcal{H}_p$ for some $p > 0$, which will be fixed in Theorem 4.1. Let Z_k , $k \in \mathbb{R}^d$, be independent centered \mathbb{C} -valued normally distributed random variables. The components of Z_k are assumed to be independent and to have variance $\gamma M_2(h)S(k)/2$. Here and in the sequel, a normally distributed random variable with variance 0 is almost surely constant. For a given $n \in \mathbb{N}$, we consider $(k_{1,r})_{r>0}, \dots, (k_{n,r})_{r>0} \in \mathbf{F} \cup \{0\}$ and set $k_i := \lim_{r \rightarrow \infty} k_{i,r}$. In view of Corollary 3.7, we assume that

$$\{k_i, -k_i\} \cap \{k_j, -k_j\} = \emptyset, \quad i \neq j. \tag{4.2}$$

Our primary interest is in the multivariate central limit theorem

$$(T_r(k_{1,r}), \dots, T_r(k_{n,r})) \xrightarrow{d} (Z_{k_1}, \dots, Z_{k_n}), \quad \text{as } r \rightarrow \infty, \tag{4.3}$$

where \xrightarrow{d} denotes convergence in distribution. In the case $d = 1$, Brillinger (see [10, Theorem 4.2]) proved that this convergence holds under a suitable assumption on the so-called (reduced) *cumulant measures* of η . We shall extend Theorem 4.2 of [10] to general dimensions, using similar methods.

To state our result, we introduce some concepts from the theory of point processes (see, e.g., [15]). For each integer m , the m -th *factorial moment measure* of η is the measure on $(\mathbb{R}^d)^m$, defined by

$$\alpha_m(\cdot) := \mathbb{E} \sum_{x_1, \dots, x_m \in \eta}^{\neq} \mathbf{1}\{(x_1, \dots, x_m) \in \cdot\}.$$

Here, \neq indicates summation over m -tuples with pairwise distinct entries. By assumption (4.1), $\alpha_m(B) < \infty$ for each bounded Borel set $B \subset (\mathbb{R}^d)^m$. If α_m has a density ρ_m with respect to Lebesgue measure on $(\mathbb{R}^d)^m$, then ρ_m is called the m -th *correlation function* of η . For $j \in [m] := \{1, \dots, m\}$, we denote by $\Pi_{m,j}$ the system of all partitions π of $[m]$ whose cardinality $|\pi|$ equals j . The m -th *factorial cumulant measure* β_m of η is the signed measure on $(\mathbb{R}^d)^m$ given by

$$\beta_m(B_1 \times \dots \times B_m) := \sum_{j=1}^m (-1)^{j-1} (j-1)! \sum_{\pi \in \Pi_{m,j}} \prod_{I \in \pi} \alpha_{|I|}(\times_{i \in I} B_i) \quad (4.4)$$

for bounded Borel sets $B_1, \dots, B_m \subset \mathbb{R}^d$. Note that β_m is only defined on bounded Borel subsets of $(\mathbb{R}^d)^m$. An equivalent definition is

$$\beta_m(B_1 \times \dots \times B_m) = \frac{\partial^m}{\partial u_1 \dots \partial u_m} \log G \left(1 + \sum_{j=1}^m u_j \mathbf{1}_{B_j} \right) \Big|_{u_1 = \dots = u_m = 0}, \quad (4.5)$$

where each of the partial derivatives is to be taken from the left. Here, the *generating functional* G of η is given by

$$G(f) := \mathbb{E} \prod_{x \in \eta} f(x)$$

for each measurable function $f: \mathbb{R}^d \rightarrow [0, \infty)$. For instance, we have $\beta_1(dx) = \gamma dx$ and

$$\beta_2(d(x, y)) = \alpha_2(d(x, y)) - \gamma^2 dx dy. \quad (4.6)$$

Assume that $m \geq 2$. Since η is stationary, β_m is invariant under joint shifts, and there exists a locally finite signed measure $\beta_m^!$ on $(\mathbb{R}^d)^{m-1}$ (the m -th reduced factorial cumulant measure of η), satisfying

$$\beta_m(\cdot) = \iint \mathbf{1}\{(x, x_1 + x, \dots, x_{m-1} + x) \in \cdot\} \beta_m^!(d(x_1, \dots, x_{m-1})) dx. \quad (4.7)$$

If $m = 2$, then (4.6) shows that (4.7) is consistent with (2.4). As in the case $m = 2$, we can introduce the *total variation measure* $|\beta_m^!|$ of $\beta_m^!$, which is a locally finite measure on $(\mathbb{R}^d)^{m-1}$.

The key assumption in this section is

$$|\beta_m^!|((\mathbb{R}^d)^{m-1}) < \infty, \quad m \geq 3. \quad (4.8)$$

Together with $|\beta_2^!|(\mathbb{R}^d) < \infty$, this condition is known as *Brillinger mixing*; see [30]. Later, we shall assume (4.8) together with (3.1), which slightly strengthens the Brillinger mixing property. In one dimension, the author of [10] makes a slightly stronger assumption (see display (2.14) in [10]).

The proof of the following central limit theorem is given in the Appendix; see Subsection 11.2.

Theorem 4.1. *Let η be a stationary point process satisfying (4.1), (3.1), and (4.8), where $(k_{1,r})_{r>0}, \dots, (k_{n,r})_{r>0} \in \mathbf{F} \cup \{\mathbf{0}\}$ satisfy (4.2) and $k_i := \lim_{r \rightarrow \infty} k_{i,r}$. Then the multivariate central limit theorem (4.3) holds.*

The following corollary is crucial for our statistical applications. It follows from Theorem 4.1 and the comments made in Example 3.2.

Corollary 4.2. *Let h be the cubic taper function from Example 3.2. Let $n \in \mathbb{N}$ and suppose that $k_1, \dots, k_n \in \mathbb{R}^d \setminus \{0\}$ satisfy (4.2). Suppose that $N_j: (0, \infty) \rightarrow \mathbb{Z}^d$, $j \in [n]$, are such that $2\pi N_j(r)/r \rightarrow k_j$ as $r \rightarrow \infty$. Then*

$$\left(T_r \left(\frac{2\pi}{r} N_1(r) \right), \dots, T_r \left(\frac{2\pi}{r} N_n(r) \right) \right) \xrightarrow{d} (Z_{k_1}, \dots, Z_{k_n}), \quad \text{as } r \rightarrow \infty. \quad (4.9)$$

Remark 4.3. Assume that η has fast decaying correlation functions of all orders, in the sense of [8, (1.10)]. It was proved in [8] (and in [53] for $d = 2$) that η is Brillinger mixing. Furthermore, the case $p = q = 1$ of [8, (1.10)], together with our assumption $\int |g_2(x) - 1| dx < \infty$, implies that $\int \|x\|^p |g_2(x) - 1| dx < \infty$ for every $p > 0$ (cf. (2.5) and (3.1)). Therefore, the assumptions of Theorem 4.1 are satisfied, and the CLT (4.3) applies. The paper [8] provides numerous examples of stationary point processes with rapidly decaying correlations. If h is the cubic taper function one might try to apply [8, Theorem 1.13] directly. Since the function f used there is subject to the same scaling as the cube, this would require an exponential function as a score function, a choice that is formally not permitted in this theorem.

We conclude the section with two general examples of stationary point processes satisfying assumption (4.8), along with the Ginibre process as a specific example.

Example 4.4. Suppose that η is a stationary *Poisson cluster process* as in [46, Exercise 8.2]; see also [15, Proposition 12.1.V]. Let \mathbb{Q} denote the cluster distribution relative to the cluster center (a probability measure on \mathbb{N}), and assume that the cluster size has moments of all orders, i.e.,

$$\int \mu(\mathbb{R}^d)^m \mathbb{Q}(d\mu) < \infty, \quad m \in \mathbb{N}. \quad (4.10)$$

Let γ_0 denote the intensity of the underlying stationary Poisson process, and let χ be a point process with distribution \mathbb{Q} . From [46, Exercise 5.6] or [15, Proposition 12.1.V], it follows that

$$\log G(1 + f) = \gamma_0 \sum_{n=1}^{\infty} \frac{1}{n!} \int \left[\mathbb{E} \sum_{x_1, \dots, x_n \in \chi}^{\neq} f(x_1 + x) \cdots f(x_n + x) \right] dx$$

for any measurable function $f: \mathbb{R}^d \rightarrow [-1, \infty)$. Let $\alpha_n^{\mathbb{Q}}$, $n \in \mathbb{N}$, denote the factorial moment measures of χ . Then, the above can be rewritten as

$$\log G(1 + f) = \gamma_0 \sum_{n=1}^{\infty} \frac{1}{n!} \int \left[\int f(x_1 + x) \cdots f(x_n + x) \alpha_n^{\mathbb{Q}}(d(x_1, \dots, x_n)) \right] dx.$$

It follows from (4.5) that the factorial cumulant measures of η are given by

$$\beta_n(\cdot) = \gamma_0 \int \mathbf{1}\{(x_1 + x, \dots, x_n + x) \in \cdot\} \alpha_n^{\mathbb{Q}}(d(x_1, \dots, x_n)) dx, \quad n \geq 2.$$

Therefore, the reduced factorial cumulant measures of η take the form

$$\beta_n^!(\cdot) = \gamma_0 \int \mathbf{1}\{(x_2 - x_1, \dots, x_n - x_1) \in \cdot\} \alpha_n^{\mathbb{Q}}(d(x_1, \dots, x_n)), \quad n \geq 2.$$

These measures are non-negative, and (4.10) ensures that $\beta_n^!((\mathbb{R}^d)^{n-1}) < \infty$. For example, suppose the points $X_{n,1}, \dots, X_{n,n}$ of χ , conditionally on $\chi(\mathbb{R}^d) = n$, are independent and identically distributed, and that $\mathbb{E}\|X_{n,2} - X_{n,1}\| \leq c$ for some constant c independent of n . Then, under assumption (4.10), a straightforward calculation shows that $\int \|x\| \beta_2^!(dx) < \infty$. In fact, it would suffice in this case to assume (4.10) only for $m = 2$.

Let $K: \mathbb{R}^d \times \mathbb{R}^d \rightarrow \mathbb{C}$ be a continuous and positive semi-definite *kernel*. Fix $\alpha \geq -1$, and assume that η is an α -*determinantal* point process with kernel K . This means that the n -th correlation functions of η are given by

$$\rho_n(x_1, \dots, x_n) = \sum_{\pi \in \Sigma_n} \alpha^{n - \#\pi} \prod_{j=1}^n K(x_j, x_{\pi(j)}), \quad x_1, \dots, x_n \in \mathbb{R}^d, \quad (4.11)$$

where Σ_n is the set of all permutations of $[n]$, and $\#\pi$ denotes the number of *cycles* in the permutation $\pi \in \Sigma_n$. In particular, we have $\rho_1(x) = K(x, x)$ and

$$\rho_2(x, y) = K(x, x)K(y, y) + \alpha |K(x, y)|^2, \quad (4.12)$$

using the symmetry $K(y, x) = \overline{K(x, y)}$. Note that α has a different meaning than in equation (1.1). We hope that this usage of well-established notation will not cause any confusion. When $\alpha = -1$, the process η is called *determinantal*. The existence of η is a non-trivial matter and can be guaranteed only for specific values of α (including $\alpha = -1$) and under additional conditions on the kernel K ; see [57, 11, 47]. Under our assumptions, the correlation functions (4.11) determine the distribution of η .

Example 4.5. Suppose that $K: \mathbb{R}^d \times \mathbb{R}^d \rightarrow \mathbb{C}$ is continuous and positive semi-definite, and satisfies $\int |K(0, x)| dx < \infty$. Since K is positive semi-definite, this implies $\int |K(0, x)|^2 dx < \infty$. Assume that η is a stationary determinantal process with kernel K . Then $K(x, x)$ is constant almost everywhere with respect to Lebesgue measure, and this constant equals the intensity γ of η . Moreover, since $\rho_2(x, y) = \rho_2(0, y - x) = \rho_2(0, x - y)$, equation (4.12) implies

$$|K(x, y)| = |K(0, y - x)| = |K(0, x - y)|. \quad (4.13)$$

It was shown in [27] (see also [5] for the case $\alpha = -1$) that η is Brillinger mixing. If $K(0, 0) > 0$, then it follows from (4.12) that the pair correlation function of η can be chosen as

$$g_2(x) = 1 + \alpha \frac{|K(0, x)|^2}{|K(0, 0)|^2}, \quad x \in \mathbb{R}^d.$$

Thus, our assumption (3.1) is equivalent to $\int \|x\|^p |K(0, x)|^2 dx < \infty$. Note that the hyperuniformity condition (2.8) means that

$$\int |K(0, x)|^2 dx = K(0, 0). \quad (4.14)$$

Example 4.6. Assume that $d = 2$, and consider the kernel

$$K(x, y) := \pi^{-1} \exp [x\bar{y} - |x|^2/2 - |y|^2/2],$$

where $x, y \in \mathbb{C}$. Let η be the *Ginibre process*, a determinantal process with kernel K ; see, e.g., [32]. It is straightforward to verify that the correlation functions (4.11) are invariant under joint shifts, so η is stationary. Moreover, we have $K(0, 0) = \pi^{-1}$ and

$$|K(x, y)|^2 = \pi^{-2} e^{-|x-y|^2}, \quad x, y \in \mathbb{C}.$$

Therefore, equation (4.14) holds, and η is hyperuniform. In addition, assumptions (3.1) and (4.8) are satisfied.

5 Asymptotic behavior of the scattering intensity

As before, let η be a stationary, locally square-integrable point process on \mathbb{R}^d that satisfies assumption (3.1). From now on, we additionally assume that η is *ergodic*; see [46, Chapter 8] for details. In this section, we focus on the scattering intensity as defined in (2.12). We fix the cubic taper function h as in Example 3.2. With this choice, equation (2.12) can be rewritten as

$$\mathcal{S}_r(k) = \frac{r^d}{\eta(W_r)} |T_r(k)|^2, \quad k \in \mathbb{R}^d, \quad (5.1)$$

where $T_r(k)$ is given in (3.10). Under assumption (3.1), Proposition 3.4 shows that $\lim_{r \rightarrow \infty} \mathbb{E}|T_r(k_r)|^2 = \gamma S(k_\infty)$, for (k_r) as in Example 3.2.

Motivated by Corollary 4.2, we introduce the following definition to control the asymptotic behavior of $\mathcal{S}_r(k_r)$. Let Z_k , for $k \in \mathbb{R}^d \setminus \{0\}$, be independent, centered, complex-valued Gaussian random variables. The real and imaginary parts of Z_k are assumed to be independent and to have variance $\gamma S(k)/2$. We call η *good* if the following condition holds for every integer n and every choice of $k_1, \dots, k_n \in \mathbb{R}^d \setminus \{0\}$ satisfying (4.2): If $N_j: (0, \infty) \rightarrow \mathbb{Z}^d$, $j \in [n]$, are such that $2\pi N_j(r)/r \rightarrow k_j$ as $r \rightarrow \infty$, then (4.9) holds.

Remark 5.1. We believe that the class of good point processes is rather large. However, rigorous results concerning the asymptotic normality of empirical Fourier transforms for general point processes remain scarce. Our Theorem 4.1 extends a result from [10] to arbitrary dimensions. The authors of [52] mention that Brillinger's approach can be extended to two dimensions, but they neither provide assumptions nor a rigorous proof. Our proof benefits from the classical work [30], where a CLT for certain shot-noise processes was established. In all of these cases, the method of cumulants is employed. This technique was also used in [8] to prove a CLT for specific functionals of point processes. Although the result in [8] does not directly apply in our setting, it includes many examples of Brillinger mixing point processes; see Remark 4.3. In the recent preprint [51], the authors establish a CLT for linear statistics of Brillinger mixing point processes, replacing the trigonometric functions $x \mapsto e^{i\langle k, x \rangle}$ with scaled versions of smooth, rapidly decaying functions. The even more recent preprint [50] derives a CLT for perturbed lattices. Both approaches again rely on the cumulant method.

Suitable mixing conditions may provide an alternative to the assumptions in Theorem 4.1. In fact, given our results of Section 3, one might apply [6, Theorem 1]. We do not pursue this direction further here.

Let E_k , for $k \in \mathbb{R}^d \setminus \{0\}$, be independent exponentially distributed random variables with mean $S(k)$. (If $S(k) = 0$, then $E_k = 0$ almost surely.) The following result highlights a key property of good point processes that is crucial for our test: the scattering intensities (2.12) converge in distribution to independent exponentially distributed random variables.

Proposition 5.2. *Assume that η is good. Let $n \in \mathbb{N}$, and let $k_1, \dots, k_n \in \mathbb{R}^d \setminus \{0\}$ satisfy (4.2). Suppose $N_j: (0, \infty) \rightarrow \mathbb{Z}^d$, $j \in \{1, \dots, n\}$, satisfy $2\pi N_j(r)/r \rightarrow k_j$ as $r \rightarrow \infty$. Then*

$$\left(\mathcal{S}_r\left(\frac{2\pi}{r}N_1(r)\right), \dots, \mathcal{S}_r\left(\frac{2\pi}{r}N_n(r)\right) \right) \xrightarrow{d} (E_{k_1}, \dots, E_{k_n}) \quad \text{as } r \rightarrow \infty.$$

Proof. Recall equation (5.1). By the spatial ergodic theorem for point processes (see [36, Corollary 10.19] or [46, Theorem 8.14]), we have $r^{-d}\eta(W_r) \rightarrow \gamma$ almost surely as $r \rightarrow \infty$. Since η is good, the continuous mapping theorem (see [36, Theorem 4.27]) implies

$$\left(\mathcal{S}_r\left(\frac{2\pi}{r}N_1(r)\right), \dots, \mathcal{S}_r\left(\frac{2\pi}{r}N_n(r)\right) \right) \xrightarrow{d} (\gamma^{-1}|Z_{k_1}|^2, \dots, \gamma^{-1}|Z_{k_n}|^2) \text{ as } r \rightarrow \infty.$$

The random variables $|Z_{k_1}|^2, \dots, |Z_{k_n}|^2$ are independent. Let X and Y be independent standard normal random variables. Using $\stackrel{d}{=}$ to denote equality in distribution, we have

$$Z_k \stackrel{d}{=} \frac{\sqrt{\gamma S(k)}}{\sqrt{2}}(X + iY).$$

Hence,

$$\frac{1}{\gamma}|Z_k|^2 \stackrel{d}{=} \frac{S(k)}{2}(X^2 + Y^2).$$

It is well known that $X^2 + Y^2$ follows an exponential distribution with mean 2, which completes the proof. \square

To support and complement the claims made in Remark 5.1, we have simulated several representative examples of both non-hyperuniform and hyperuniform point processes:

- (i) The stationary Poisson process; see [46].
- (ii) A Poisson cluster process, as described in Example 4.4. This process is characterized by the following properties. Starting from a realization of a homogeneous Poisson point process, each point serves as the center of a cluster. The clusters are independent and identically distributed, centered at these “parent points”, and consist of a Poisson-distributed number of “children” points. Each child is drawn from a centered normal distribution in \mathbb{R}^d with identity covariance matrix (wrapped up on the torus). The resulting point process, which includes only the children and not the parents, is known as the (modified) *Thomas process*. In our simulations, the mean number of points per cluster is set to 10.

- (iii) A *random adsorption process* (RSA) close to saturation; see [64]. Realizations are generated by sequentially placing spheres (or intervals/disks in lower dimensions) randomly into space under a non-overlap constraint. We use the simulation procedure described in [64], conditioning on a fixed number of points per sample, which determines the volume fraction of the non-overlapping spheres. The volume fractions used are 74.7% for $d = 1$, 54.7% for $d = 2$, and 38.4% for $d = 3$.
- (iv) The uniformly randomized lattice (URL), see [39]. In this model, each point of a stationarized lattice is independently shifted within its corresponding unit cell, producing a stationary point process.
- (v) Matching of the lattice \mathbb{Z}^d with a Poisson process of intensity $\rho > 1$ [40]. The matched Poisson points form a hyperuniform point process. In our simulation, we choose $\rho = 3.0$.

The processes described in (i)-(iii) are non-hyperuniform, whereas those in (iv) and (v) exhibit hyperuniformity. In the latter two models, the lattice is stationarized, i.e., it is shifted by a random vector uniformly distributed in the cube $[0, 1)^d$. Remarkably, in both cases, the asymptotic exponential distribution of the scattering intensity is achieved with striking accuracy even at relatively small system sizes (see below).

Remark 5.3. The processes listed in (i), (ii) and (iv) satisfy our general assumption (3.1); in fact, the stronger assumption (1.2) holds in each case. (For the Poisson cluster process, this requires a suitable moment assumption.) The same applies to the RSA process in (iii), although a formal proof does not yet appear to exist in the literature. A perturbed lattice, by contrast, does not generally satisfy condition (2.6). To ensure that a perturbed lattice fulfills (2.6), the perturbation must be chosen in a specific way, a property shared by the URL model; see [39] for details. If the perturbation is isotropic and has a finite second moment, then (1.1) holds for $\alpha = 2$ in a neighborhood of the origin. For the matching process, (2.6) does not hold, at least not in the stationary version used here. Nevertheless, the structure factor is well-defined for each wave vector outside the reciprocal lattice of \mathbb{Z}^d . According to [40, Proposition 8.1], the stationarized matching process possesses a pair correlation function g_2 . However, we expect that $|g_2 - 1|$ is not integrable, implying that condition (2.6) fails. Still, we presume that the structure factor is well-defined for wave vectors outside the reciprocal lattice of \mathbb{Z}^d .

The point processes described above were simulated in each spatial dimension $d \in \{1, 2, 3\}$ at unit intensity $\gamma = 1$, using periodic boundary conditions, i.e., on the flat torus. Based on these simulations, we computed the scattering intensity $\mathcal{S}_r(k)$, as defined in (2.12), for a variety of wave vectors (see below). Since the theoretical distribution function of $\mathcal{S}_r(k)$ is not explicitly known, we generated one million independent realizations of each point process — per model, per dimension, and for each wave vector considered. Let $\overline{\mathcal{S}}_r(k)$ denote the arithmetic mean of the 10^6 realizations of $\mathcal{S}_r(k)$. We then computed the empirical distribution function $F_{r,k}$ (say) of the normalized values $\mathcal{S}_r(k)/\overline{\mathcal{S}}_r(k)$. That is, for each $z > 0$, $F_{r,k}(z)$ gives the relative frequency of the 10^6 realizations of $\mathcal{S}_r(k)/\overline{\mathcal{S}}_r(k)$ that are less than or equal to z . In Figure 2, we plot the *complementary* empirical distribution function $F_{r,k}^c := 1 - F_{r,k}$, and, for simplicity, we denote this by $F^c = F_{r,k}^c$.

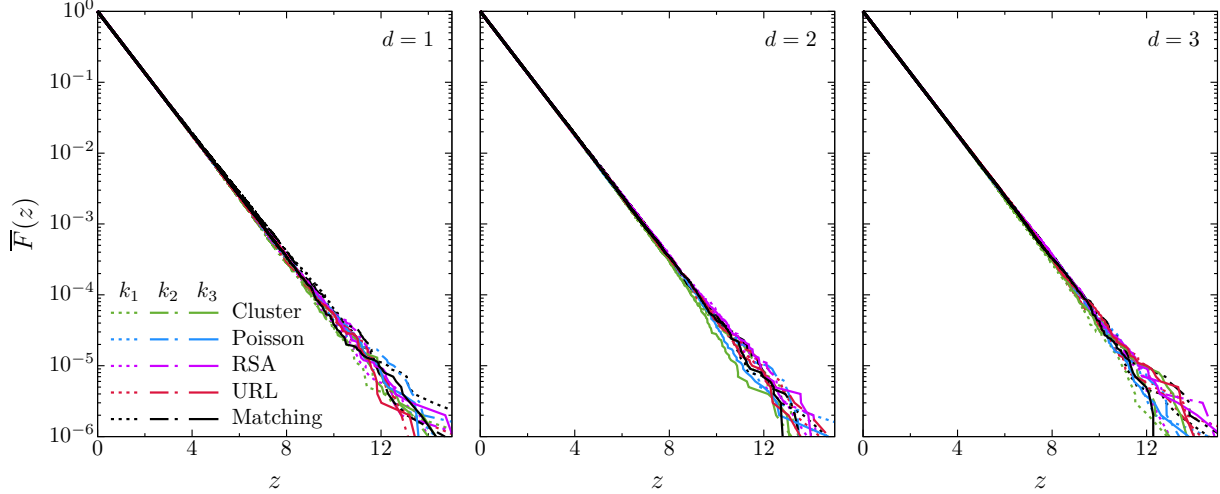


Figure 2: Empirical complementary distribution function F^c of the normalized scattering intensity $\mathcal{S}(k)/\overline{\mathcal{S}}(k)$.

The observation window is the cube $[0, L]^d$, where L is the standard notation for the system size in the applied literature. In our previous notation, this corresponds to r . We use $\mathcal{S}(k)$ as shorthand for $\mathcal{S}_r(k) = \mathcal{S}_L(k)$. Throughout, we have chosen the number density to be 1, corresponding to an expected number of L^d points in $[0, L]^d$. Remarkably, we worked with relatively small system sizes. More precisely, the expected number of points per sample is 1000 for $d = 1$, 1225 for $d = 2$, and again 1000 for $d = 3$. In view of the lattice-based models (iv) and (v), these numbers were chosen to be integer powers of d . To accommodate the periodic boundary conditions, we slightly modified the matching process (v) by performing it on the torus. Theorem 5.1 in [40] strongly suggests that the difference between this torus-based model and the restriction of the original model to $[0, L]^d$ vanishes as $L \rightarrow \infty$. This modification requires a corresponding adaptation of assumption (4.9): namely, the restriction of η to W_r (which determines T_r) must be replaced by the set of matched points on the torus. In principle, this same consideration applies to models (ii)-(iv). For simplicity, the data shown in Figure 2 are restricted to three distinct wave vectors per dimension. Setting $\tau := 2\pi/L$, the selected wave vectors are:

- $k_1 = \tau$, $k_2 = 158\tau$, $k_3 = 317\tau$ if $d = 1$,
- $k_1 = \tau \times (0, 1)$, $k_2 = \tau \times (6, 0)$, $k_3 = \tau \times (8, 8)$ if $d = 2$,
- $k_1 = \tau \times (0, 1, 0)$, $k_2 = \tau \times (2, 2, 2)$, $k_3 = \tau \times (3, 0, 0)$ if $d = 3$.

According to Proposition 5.2 and the normalization $\mathcal{S}(k) \mapsto \mathcal{S}(k)/\overline{\mathcal{S}}(k)$, the complementary empirical distribution function F^c is expected to approximate the reciprocal exponential function, i.e., the complementary distribution function of a unit-rate exponential distribution. In this regard, Figure 2 is illustrative: on a logarithmic scale, the figure shows the empirical complementary distribution function F^c of the scattering intensity for dimensions $d = 1$ (left), $d = 2$ (middle), and $d = 3$ (right). Due to the normalization, all curves for F^c collapse onto a single one, independent of the specific model or wave vector chosen. Moreover, in each case, the agreement with an exponential distribution is

remarkably accurate. This close correspondence was also observed for many additional wave vectors not shown here. Small fluctuations of $F^c(z)$ on the order of 10^{-6} , visible only at large values of $\mathcal{S}(k)/\overline{\mathcal{S}}(k)$, are consistent with purely statistical variation across our 10^6 samples; we observe no systematic deviations from the exponential distribution.

Finally, our results indicate only a weak correlation between $\mathcal{S}(k)$ values for different wave vectors k . Even for neighboring wave vectors close to the origin in Fourier space, the correlation coefficient remains consistently below 0.02. This observation aligns perfectly with Proposition 5.2.

6 Maximum likelihood estimation

In this section, we adopt an asymptotic framework naturally suggested by Proposition 5.2. Within this setting, the background of point processes becomes irrelevant, and our starting point is the multivariate asymptotic distribution of scattering intensities provided by that proposition. This framework allows us to define maximum likelihood estimators for a parameterized structure factor. Specifically, we employ the expansion (1.1) of $S(k)$ as $k \rightarrow 0$. While this expansion introduces an additional approximation, it is justified by the fact that (1.1) holds in the same asymptotic regime of large system sizes, where small wave vectors become accessible.

To proceed, consider n wave vectors $k_1, \dots, k_n \in \mathbb{R}^d \setminus \{0\}$ satisfying condition (4.2). Define $\kappa_j := \|k_j\|^\alpha$ for $j \in [n]$. In a slight abuse of prior notation, let X_1, \dots, X_n be independent exponentially distributed random variables with expectations $\mathbb{E}(X_j) = s + t\kappa_j$ for $j \in [n]$, where $s \geq 0$ and $t \in \mathbb{R}$ are unknown parameters to be estimated from observed realizations x_1, \dots, x_n of X_1, \dots, X_n . This statistical problem is of interest in its own right. Formally, the parameter space is defined as

$$\begin{aligned} \Theta &:= \{(s, t) \in \mathbb{R}^2 : s \geq 0, s + t\kappa_1 > 0, \dots, s + t\kappa_n > 0\} \\ &= \left\{ (s, t) \in \mathbb{R}^2 : s \geq 0, t > -\frac{s}{\max(\kappa_1, \dots, \kappa_n)} \right\}, \end{aligned}$$

which describes a cone in the (s, t) -plane. For $(s, t) \in \Theta$, let $\mathbb{P}_{s,t}$ denote the probability measure governing the random variables X_1, \dots, X_n , with corresponding expectation and variance operators $\mathbb{E}_{s,t}$ and $\text{Var}_{s,t}$, respectively. This notation omits the dependence on n and on the specific wave vectors k_1, \dots, k_n for simplicity. We formulate the null hypothesis H_0 as the condition of hyperuniformity. In light of the asymptotic regime and the constraint from (1.1), this corresponds to the subset $\Theta_0 := \{(s, t) \in \Theta : s = 0\}$ of Θ .

Under $\mathbb{P}_{s,t}$, the density of X_j (for each $j \in [n]$) is given by

$$y \mapsto \frac{1}{s + t\kappa_j} \exp\left(-\frac{y}{s + t\kappa_j}\right), \quad y \geq 0.$$

Given observed positive values x_1, \dots, x_n , the corresponding log-likelihood function is

$$\mathcal{L}(x_1, \dots, x_n; s, t) = \sum_{j=1}^n \left[-\log(s + t\kappa_j) - \frac{x_j}{s + t\kappa_j} \right]. \quad (6.1)$$

We begin by considering the maximum likelihood (ML) estimation of t under the null hypothesis H_0 .

6.1 Estimation under H_0

Under $\mathbb{P}_{0,t}$, that is, under the constraint $s = 0$ imposed by H_0 , the log-likelihood function simplifies to

$$\mathcal{L}(x_1, \dots, x_n; 0, t) = -n \log t - \frac{1}{t} \sum_{j=1}^n \frac{x_j}{\kappa_j} - \sum_{j=1}^n \log \kappa_j.$$

The first and second derivatives with respect to t are given by

$$\begin{aligned} \frac{\partial \mathcal{L}}{\partial t}(x_1, \dots, x_n; 0, t) &= -\frac{n}{t} + \frac{1}{t^2} \sum_{j=1}^n \frac{x_j}{\kappa_j}, \\ \frac{\partial^2 \mathcal{L}}{\partial t^2}(x_1, \dots, x_n; 0, t) &= \frac{n}{t^2} - \frac{2}{t^3} \sum_{j=1}^n \frac{x_j}{\kappa_j}. \end{aligned}$$

Define the function $h_0: (0, \infty)^n \rightarrow \mathbb{R}$ by

$$h_0(x_1, \dots, x_n) := \sup\{\mathcal{L}(x_1, \dots, x_n; 0, t) : (0, t) \in \Theta\}. \quad (6.2)$$

Then the ML estimate $\hat{t}_0 \equiv \hat{t}_0(x_1, \dots, x_n)$ of t based on x_1, \dots, x_n is uniquely determined by the condition $\mathcal{L}(x_1, \dots, x_n; 0, \hat{t}_0) = h_0(x_1, \dots, x_n)$, and it takes the explicit form

$$\hat{t}_0(x_1, \dots, x_n) = \frac{1}{n} \sum_{j=1}^n \frac{x_j}{\kappa_j}. \quad (6.3)$$

Recall that the *gamma distribution* with shape parameter a and scale parameter b has the density

$$y \mapsto \mathbf{1}\{y \geq 0\} \frac{b^a y^{a-1} e^{-by}}{\Gamma(a)}.$$

Under $\mathbb{P}_{0,t}$, the estimator $\hat{t}_0(X_1, \dots, X_n)$ is the average of n independent exponential random variables with mean t . By a standard convolution property of the gamma distribution, it follows that $\hat{t}_0(X_1, \dots, X_n)$ is gamma-distributed with shape parameter $a = n$ and scale parameter $b = n/t$. Consequently,

$$\mathbb{E}_{0,t}(\hat{t}_0(X_1, \dots, X_n)) = \frac{a}{b} = t, \quad \text{Var}_{0,t}(\hat{t}_0(X_1, \dots, X_n)) = \frac{a}{b^2} = \frac{t^2}{n},$$

showing that $\hat{t}_0(X_1, \dots, X_n)$ is an unbiased and consistent estimator of t . In the following, we often abuse notation slightly by writing \hat{t}_0 in place of $\hat{t}_0(X_1, \dots, X_n)$; its meaning will be clear from the context. We will adopt similar shorthand for two additional estimators introduced below.

In all our simulations, a cubic taper function is used, as is common in physics. In accordance with Corollary 4.2, we select the wave vectors from the reciprocal lattice associated with a periodic simulation box of side length L . Specifically, we choose the following *commensurable* wave vectors:

$$K_L := \left\{ k \in \frac{2\pi}{L} \times \mathbb{Z}^d \setminus \{0\} : \|k\| < k_{<} \right\}. \quad (6.4)$$

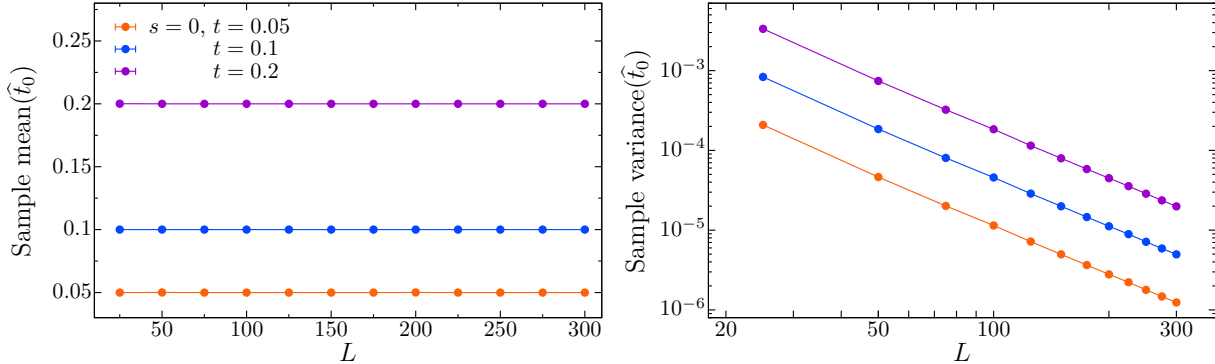


Figure 3: Unbiasedness and consistency of \hat{t}_0 are demonstrated by plots of the sample mean value (left) and variance (right) as functions of the linear system size L .

In our experiments for the asymptotic setting, we take $d = 2$ and $k_{<} = 0.75$. Other choices of d and $k_{<}$ yield qualitatively similar results, with differences arising primarily in the speed of convergence, as expected. Note that in the asymptotic setting the choice of L (only) determines which wave vectors are chosen for the simulations. Note also that, for fixed $k_{<}$, the number $n = |K_L|$ of wave vectors increases with L .

Figure 3 illustrates the unbiasedness and consistency properties of the estimator \hat{t}_0 for three different values of t . The left-hand panel displays the sample means as estimators $\widehat{\mathbb{E}}(\hat{t}_0)$ of the expectation, while the right-hand panel shows the sample variances as estimators $\widehat{\mathbb{V}\text{ar}}(\hat{t}_0)$ of the variance. For each choice of the parameters t and L , the estimates are based on 10^6 independent realizations of (X_1, \dots, X_n) . In the case $s = 0$ and $L = 100$, Figure 4 presents the corresponding histograms as density estimates for \hat{t}_0 , which align very well with the fitted gamma distributions. Typically, histograms use vertical bars whose areas represent frequency counts over a fixed range. In our visualizations, however, we adopt a modified representation using bullets instead of columns. Each interval forming the histogram base has equal length. The horizontal coordinates of a bullet represents the midpoint of its base, while its height corresponds to the relative frequency of data within that interval, divided by the base length. Thus, the bullet heights serve as density estimates for \hat{t}_0 at those midpoints. These conventions also apply, mutatis mutandis, to all subsequent figures displaying histograms.

6.2 Estimation in the full parameter space

When s and t are allowed to vary freely within Θ , we cannot explicitly maximize (6.1). However, since Θ is a cone in the (s, t) -plane, the problem of maximizing a function of two variables can be reduced to a univariate optimization problem. To simplify the notation, we omit the dependence on x_1, \dots, x_n in the log-likelihood function. For $(s, t) \in \Theta$ and $\delta > 0$, we have

$$\mathcal{L}(\delta s, \delta t) = \mathcal{L}(s, t) - n \log \delta + \left(1 - \frac{1}{\delta}\right) \sum_{j=1}^n \frac{x_j}{s + t\kappa_j}.$$

Therefore, it is natural to substitute $s =: \delta \cos \vartheta$ and $t =: \delta \sin \vartheta$, where $\delta > 0$, $\vartheta \in (\vartheta_0, \pi/2]$, and ϑ_0 is defined by $\tan \vartheta_0 = -1/\max(\kappa_1, \dots, \kappa_n)$. For the moment, we tem-

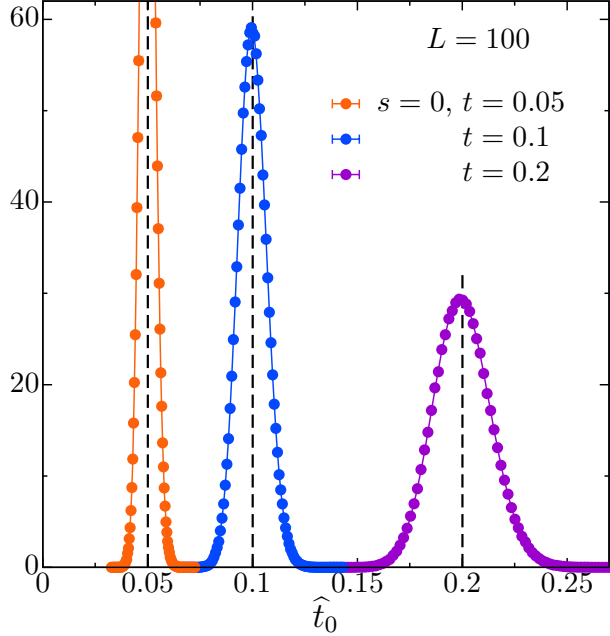


Figure 4: Density estimates for \hat{t}_0 (bullets) and densities of gamma distributions with the same expectation and variance (solid lines).

porarily exclude the case $(s, t) = (0, 0)$. Notice that

$$\frac{d}{d\delta} \mathcal{L}(\delta \cos \vartheta, \delta \sin \vartheta) = -\frac{n}{\delta} + \frac{1}{\delta^2} \sum_{j=1}^n \frac{x_j}{\cos \vartheta + \kappa_j \sin \vartheta}, \quad \delta > 0.$$

This derivative vanishes if and only if

$$\delta = \delta_0(\vartheta) := \frac{1}{n} \sum_{j=1}^n \frac{x_j}{\cos \vartheta + \kappa_j \sin \vartheta}.$$

Assume that $\delta_0(\vartheta) > 0$. Since $\frac{d}{d\delta} \mathcal{L}(\delta \cos \vartheta, \delta \sin \vartheta)$ is positive for $\delta < \delta_0(\vartheta)$ and negative for $\delta > \delta_0(\vartheta)$, the function $(0, \infty) \ni \delta \mapsto \mathcal{L}(\delta \cos \vartheta, \delta \sin \vartheta)$ attains a unique maximum at $\delta = \delta_0(\vartheta)$. Defining

$$\mathcal{L}^*(\vartheta) := \max_{\delta \geq 0} \mathcal{L}(\delta \cos \vartheta, \delta \sin \vartheta), \quad (6.5)$$

and substituting $\delta_0(\vartheta)$ into the definition of $\mathcal{L}(\delta s, \delta t)$, we obtain

$$\mathcal{L}^*(\vartheta) = \mathcal{L}(\delta_0(\vartheta) \cos \vartheta, \delta_0(\vartheta) \sin \vartheta). \quad (6.6)$$

This remains true if $\delta_0(\vartheta) = 0$ or, equivalently, if $x_1 = \dots = x_n = 0$. This case is of no practical relevance and will be excluded in the sequel. We will maximize \mathcal{L} by first maximizing \mathcal{L}^* . Some properties of \mathcal{L}^* are discussed in Appendix 11.3.

Similarly to (6.2), we define a function h_1 on $(0, \infty)^n$ by

$$h_1(x_1, \dots, x_n) := \sup\{\mathcal{L}(x_1, \dots, x_n; s, t) : (s, t) \in \Theta\}. \quad (6.7)$$

Given (x_1, \dots, x_n) , let $\widehat{\Theta}(x_1, \dots, x_n)$ denote the set of all $(s', t') \in \Theta$ such that

$$\mathcal{L}(x_1, \dots, x_n; s', t') = h_1(x_1, \dots, x_n).$$

By Lemma 11.2, the set $\widehat{\Theta}(x_1, \dots, x_n)$ is non-empty.

Remark 6.1. Let $(x_1, \dots, x_n) \in (0, \infty)^n$. Our numerical analysis and Lemma 11.2 strongly suggest that \mathcal{L}^* has a unique maximizer $\widehat{\vartheta}(x_1, \dots, x_n)$, that is

$$\{\vartheta' : \mathcal{L}^*(\vartheta') = \max_{\vartheta_0 < \vartheta \leq \pi/2} \mathcal{L}^*(\vartheta)\} = \{\widehat{\vartheta}(x_1, \dots, x_n)\}. \quad (6.8)$$

Then the original likelihood function \mathcal{L} has a unique maximizing pair $(\widehat{s}, \widehat{t}_1)$ (depending on the data) given by

$$\widehat{s} = \widehat{\delta} \cos \widehat{\vartheta}, \quad (6.9)$$

$$\widehat{t}_1 = \widehat{\delta} \sin \widehat{\vartheta}, \quad (6.10)$$

where

$$\widehat{\delta} := \delta_0(\widehat{\vartheta}) = \frac{1}{n} \sum_{j=1}^n \frac{x_j}{\cos \widehat{\vartheta} + \kappa_j \sin \widehat{\vartheta}}.$$

Whenever we use the notation $\widehat{s}(\cdot)$ and $\widehat{t}_1(\cdot)$, we implicitly assume (6.8).

Before discussing the findings of our simulations, we present two useful invariance properties.

Lemma 6.2. *Let $t > 0$. Then*

$$\begin{aligned} & \mathbb{P}_{0,t}(h_1(X_1, \dots, X_n) - h_0(X_1, \dots, X_n) \in \cdot) \\ &= \mathbb{P}_{0,1}(h_1(X_1, \dots, X_n) - h_0(X_1, \dots, X_n) \in \cdot). \end{aligned}$$

Proof. The parameter space Θ is invariant under positive scaling. Furthermore, the log-likelihood function is essentially scale-invariant, since

$$\mathcal{L}(rx_1, \dots, rx_n; rs, rt) = \mathcal{L}(x_1, \dots, x_n; s, t) - n \log r,$$

for any $r > 0$, any $(s, t) \in \Theta$, and any $(x_1, \dots, x_n) \in (0, \infty)^n$. It follows that

$$h_1(rx_1, \dots, rx_n) - h_0(rx_1, \dots, rx_n) = h_1(x_1, \dots, x_n) - h_0(x_1, \dots, x_n).$$

Now, set $r := t^{-1}$, and note the distributional identity

$$\mathbb{P}_{0,t}((t^{-1}X_1, \dots, t^{-1}X_n) \in \cdot) = \mathbb{P}_{0,1}((X_1, \dots, X_n) \in \cdot),$$

which completes the proof. \square

If assumption (6.8) holds, the following corollary implies that

$$\mathbb{P}_{0,t}(\widehat{s}(X_1, \dots, X_n) = 0) = \mathbb{P}_{0,1}(\widehat{s}(X_1, \dots, X_n) = 0), \quad t > 0.$$

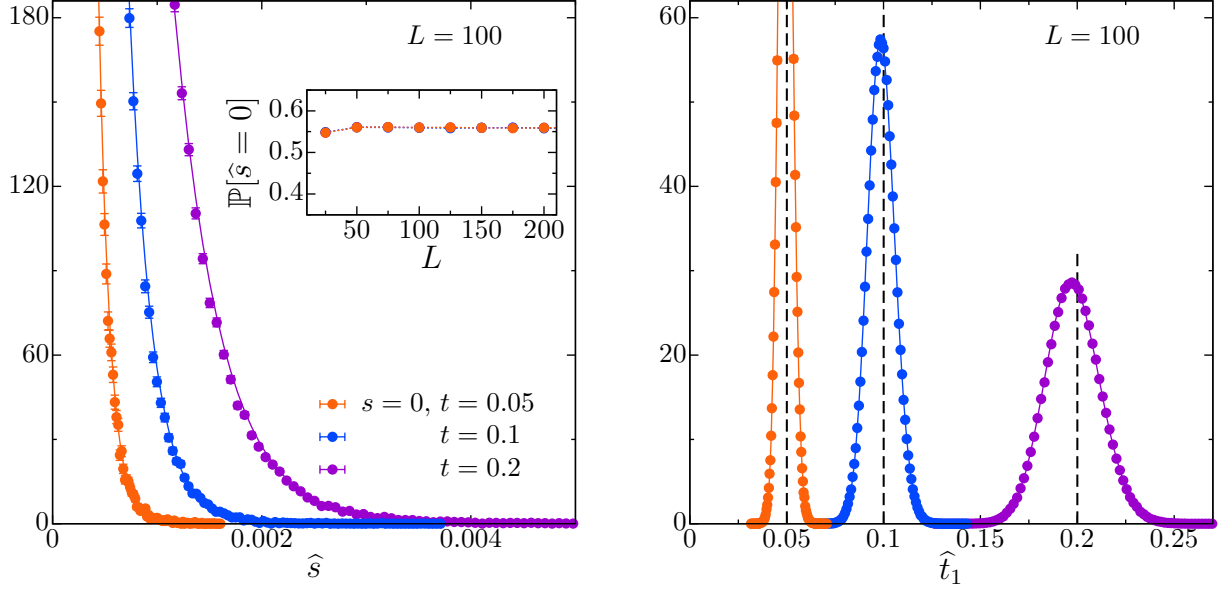


Figure 5: Density estimates for the continuous part of \hat{s} and for \hat{t}_1 (bullets) and densities of gamma distributions with the same expectation and variance (solid lines). The inset shows the size of the atom of \hat{s} as a function of L .

Corollary 6.3. *Let $t > 0$. Then*

$$\mathbb{P}_{0,t}(\hat{\Theta}(X_1, \dots, X_n) \cap \Theta_0 = \emptyset) = \mathbb{P}_{0,1}(\hat{\Theta}(X_1, \dots, X_n) \cap \Theta_0 = \emptyset).$$

Proof. Let $(x_1, \dots, x_n) \in (0, \infty)^n$, and suppose that $\hat{\Theta}(x_1, \dots, x_n) \cap \Theta_0 \neq \emptyset$. Then, by definition, we immediately obtain $h_0(x_1, \dots, x_n) = h_1(x_1, \dots, x_n)$. Conversely, assume that the above identity holds. As shown earlier, there exists some $\hat{t}_0 > 0$ such that $\mathcal{L}(x_1, \dots, x_n; 0, \hat{t}_0) = h_0(x_1, \dots, x_n)$. Hence, $(0, \hat{t}_0) \in \hat{\Theta}(x_1, \dots, x_n)$, implying that $\hat{\Theta}(x_1, \dots, x_n) \cap \Theta_0 \neq \emptyset$. The assertion then follows directly from Lemma 6.2. \square

We numerically optimize $\mathcal{L}(x_1, \dots, x_n; s, t)$ to machine precision, using a tolerance of about 10^{-14} . Such high accuracy is essential for reliably studying the $\mathbb{P}_{s,t}$ -distribution of $\hat{s}(X_1, \dots, X_n)$, especially since the density of its continuous part diverges as $s \rightarrow 0$, as suggested by simulations.

Using the commensurable wave vectors K_r from (6.4), i.e., the same wave vectors as for Figures 3 and 4, we repeat the optimization for 10^6 independent simulations of the vector of (X_1, \dots, X_n) for each choice of s, t , and L . We then approximate the densities of $\hat{s}(X_1, \dots, X_n)$ and $\hat{t}_1(X_1, \dots, X_n)$ using histograms of the simulation results. See Figures 5 and 6 for simulations with $s = 0$ and $s > 0$, respectively. The inset in Figure 5 and the left panel in Figure 6 illustrate the stabilization of the atom's mass. Asymptotic unbiasedness and consistency are demonstrated in Figures 7 and 8.

Our simulations strongly suggest the following asymptotic behavior of our estimators:

- The estimators are consistent and asymptotically unbiased.
- The asymptotic distribution of $\hat{s}(X_1, \dots, X_n)$, as $L \rightarrow \infty$, includes an atom at the origin. The atom mass $\mathbb{P}_{s,t}(\hat{s}(X_1, \dots, X_n) = 0)$ converges to zero if $s > 0$, and to

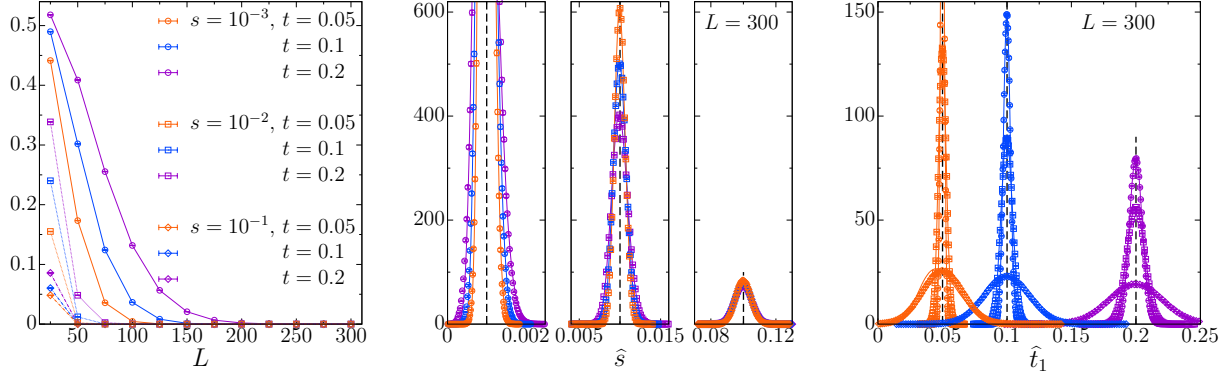


Figure 6: The non-hyperuniform case: (left) the size of the atom of \widehat{s} ; (center and right) density estimates for \widehat{s} and \widehat{t}_1 (bullets) and densities of gamma distributions with the same expectation and variance (solid lines).

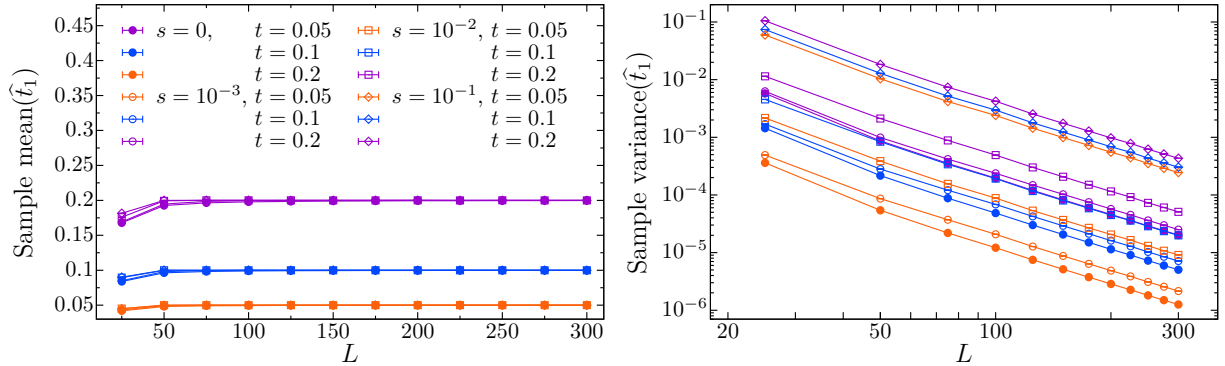


Figure 7: Asymptotic unbiasedness and consistency of \widehat{t}_1 are illustrated by plots of the sample mean value (left) and variance (right) as functions of the linear system size L .

a constant (independent of t) if $s = 0$. This t -independence follows from Corollary 6.3.

- As $L \rightarrow \infty$, the continuous parts of the distributions of both $\widehat{s}(X_1, \dots, X_n)$ and $\widehat{t}_1(X_1, \dots, X_n)$ converge to gamma distributions. For $s = 0$, these gamma approximations are already accurate at relatively small system sizes.

7 Likelihood ratio test for hyperuniformity

In this section, we adopt the framework established in Section 6. We define the test statistic

$$T(x_1, \dots, x_n) := 2[h_1(x_1, \dots, x_n) - h_0(x_1, \dots, x_n)], \quad (x_1, \dots, x_n) \in (0, \infty)^n, \quad (7.1)$$

where h_0 and h_1 are defined in (6.2) and (6.7), respectively. By construction, T is nonnegative. Under our hypothesis (6.8), we have $T(x_1, \dots, x_n) = 0$ if and only if $\widehat{s}(x_1, \dots, x_n) = 0$. Hence, the $\mathbb{P}_{s,t}$ -atom of $\widehat{s}(X_1, \dots, X_n)$ carries over to the distribution of $T(X_1, \dots, X_n)$.

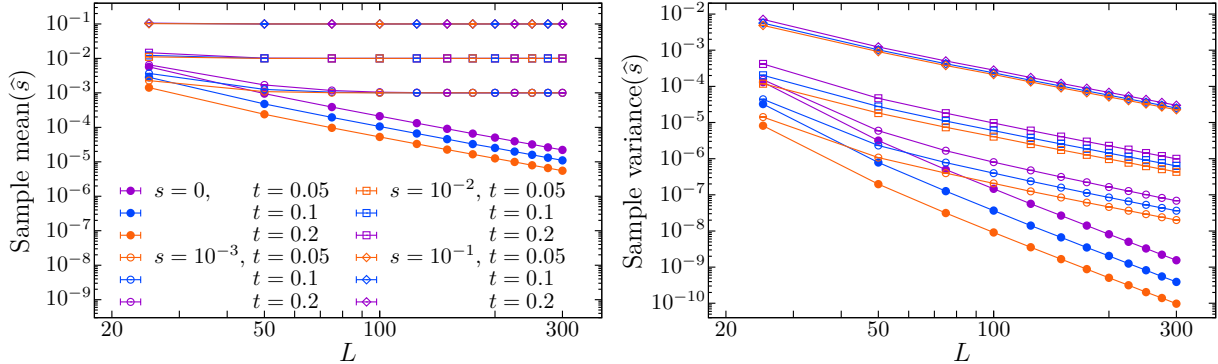


Figure 8: Asymptotic unbiasedness and consistency of \hat{s} are demonstrated by plots of the mean value (left) and variance (right) as functions of L .

Figure 9 presents the simulation results for the test statistic T , specifically showing the atom size and density estimates for the continuous part of T . The same set of samples is used to compute T for Fig. 9 and (\hat{s}, \hat{t}_1) for Fig. 5.

Based on the simulation results shown in Fig. 9, we conjecture that, as $n \rightarrow \infty$, the limiting distribution of T under H_0 is a mixture of an atom at 0 and a gamma distribution with parameters $a = k/2$ and $b = 1/2$, where k is slightly less than 1. For $k = 1$, this would correspond to a χ^2 -distribution with one degree of freedom. In our case, we refer to this limiting form as a χ^2 -distribution with *fractional* parameter k . Therefore, we assume in the following that the limiting distribution of T consists of an atom of size 0.5585 and a continuous part with fractional parameter $k = 0.9400$. Importantly, this approximation holds well even for small system sizes, and it implies that the asymptotic distribution of T does not depend on t . In fact, this t -independence follows directly from Lemma 6.2. The existence of an universal (i.e., t -independent) explicit limit distribution for T is crucial for our statistical test of hyperuniformity.

Under H_1 , the distribution of T is asymptotically (as $n \rightarrow \infty$) well approximated by a gamma distribution; see Figure 10, which is based on the same simulation settings as in Section 6.2 but extended to additional values of s , t , and L . Moreover, we find that the distribution of T can be well approximated using only a single parameter, i.e., a scatter plot of a and b collapses onto a single curve.

8 Testing hyperuniformity in an example

We conclude by demonstrating the practical relevance and remarkable sensitivity of the novel test through its application to model (v) of matched points, as introduced in Section 5. This model is particularly advantageous: although it exhibits non-trivial correlations, it is known to be hyperuniform [40]. Furthermore, it allows for efficient simulation of large samples, and the parameter t can be conveniently tuned by adjusting the intensity ρ . While our simulations focus on two-dimensional systems, the results are, in principle, applicable in any spatial dimension.

We first verify that the approximations developed in previous sections remain highly accurate for realistically sized systems commonly encountered in applications; see [59] and references therein. Figure 11 displays the empirical probability density of the test

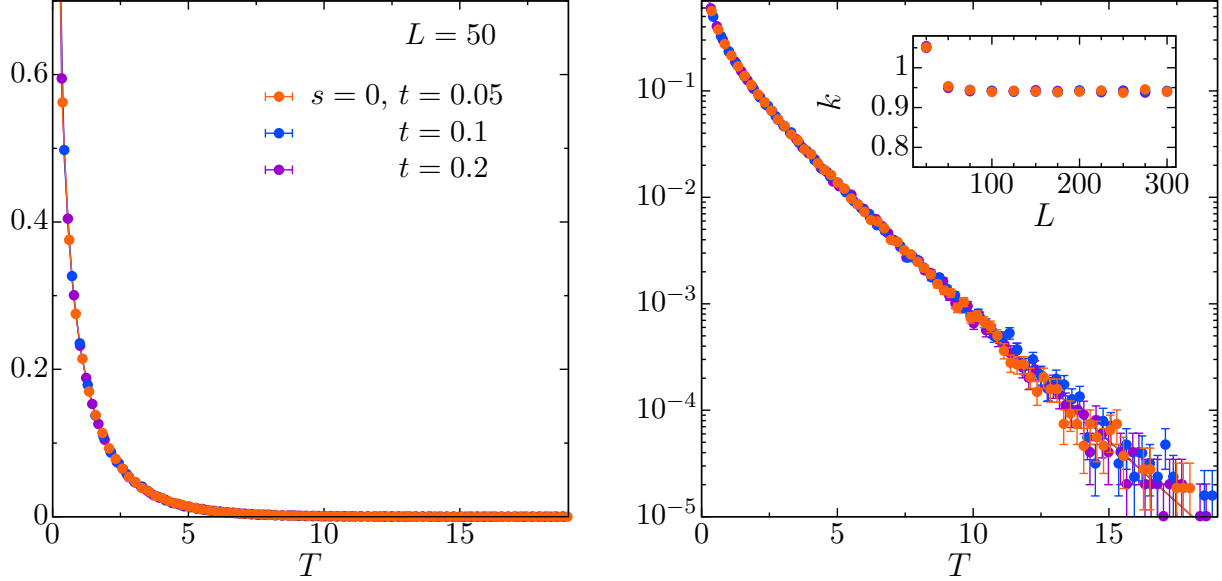


Figure 9: Density estimates for the continuous part of T (bullets) in our asymptotic framework, i.e., for exponentially distributed and independent values of $S(k)$ with $s = 0$, and densities of a χ^2 -distribution with the same expectation (solid lines). A linear plot is shown on the left-hand side, and a log-log plot on the right-hand side. The inset shows the *fractional* parameter k of the χ^2 -distribution as a function of L .

statistic T for various values of t . In all cases, the empirical distributions collapse onto the predicted χ^2 -distributions, within statistical error margins. The insets of Figure 11 plot the two defining parameters of the limiting distribution, namely, the atom size and the ‘fractional degree of freedom’, as functions of the linear system size L . The data obtained from simulations (indicated by bullets) closely match the asymptotic predictions (represented by horizontal lines).

The specific simulation parameters are as follows. The maximum length of the wave vectors is adapted to the value of ρ , ensuring that the parabolic approximation remains valid with sufficient accuracy (see the following two paragraphs for discussion). Specifically, the parameter $k_{<}$ in equation (6.4) is set to 0.50 for $\rho = 3.0$ (corresponding to $t \approx 0.05$), 0.40 for $\rho = 2.5$ ($t \approx 0.07$), and 0.33 for $\rho = 2.0$ ($t \approx 0.09$). These are heuristic choices, and our results are not sensitive to moderate variations in $k_{<}$. The test statistic T is computed independently for each sample. The number of independent realizations per system size is: 1 000 000 for $L = 50$, 400 000 for $L = 75$, 200 000 for $L = 100$, 100 000 for $L = 125$, 80 000 for $L = 150$, 60 000 for $L = 175$, and 40 000 for $L = 200$.

An general challenge in any numerical study of hyperuniformity lies in ensuring that sample sizes are large enough to reveal the asymptotic scaling behavior of the structure factor (or equivalently, the number variance). For the matching process in particular, the onset of the hyperuniform scaling regime depends on the value of ρ . As ρ approaches one, the range of wavenumbers over which the hyperuniform scaling $S(k) \sim k^2$ holds diminishes; see Figure 9 in [40] and Figure 10 for a corresponding analysis based on the number variance. Once the system size becomes sufficiently large, we observe a class I hyperuniform scaling with $\alpha = 2$, consistent with Remark 8.3 in [40].

It is important to note that our test remains valid even for smaller system sizes or larger

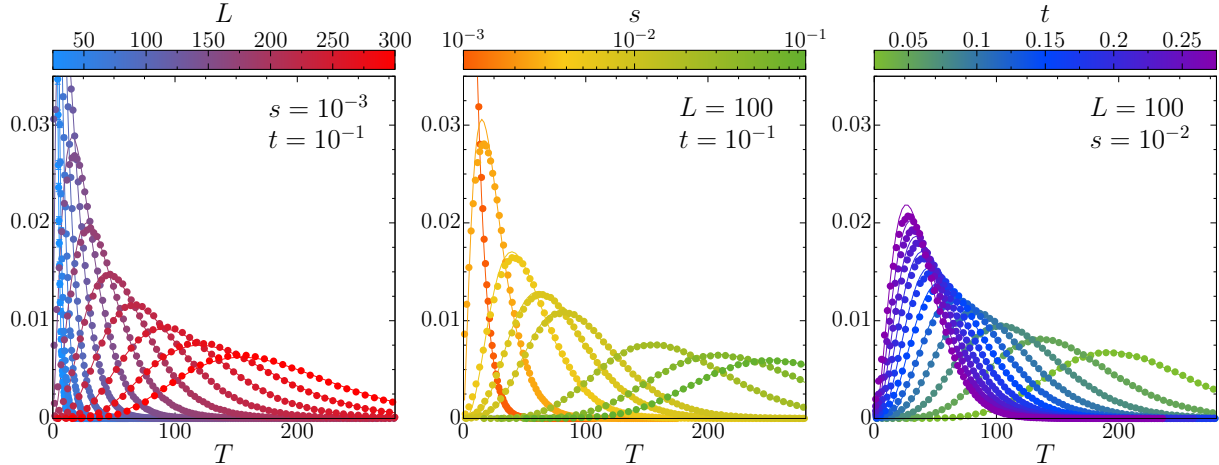


Figure 10: Density estimates for the continuous part of T in our asymptotic framework, but now with different values of s , t , and L .

wavenumber ranges where the structure factor deviates from the parabolic approximation. In such cases, rejection of the null hypothesis may occur solely due to the incorrect functional form of $S(k)$. For this reason, the test should also correctly reject class II and class III hyperuniform systems, which are characterized by different asymptotic scaling laws [59]. This limitation exemplifies a broader statistical issue; rejection of the null hypothesis does not necessarily imply non-hyperuniformity, but may rather indicate a departure from a specific scaling assumption.

Despite these caveats, we find our test to be robust against small deviations from the approximation (1.1). In fact, (1.1) may not strictly hold for the matching process, since the underlying lattice introduces anisotropy. Nevertheless, the simulations strongly suggest that $S(k)$ is effectively isotropic, except at the wave vectors of the reciprocal lattice of \mathbb{Z}^d . As a result, the distribution of T is indistinguishable from the asymptotic distribution under the null hypothesis H_0 , as illustrated in Figure 11.

Next, we employ independent thinning to continuously vary the value of $S(0)$. Given $p \in [0, 1]$ and a stationary point process η , the p -thinning η_p of η is defined by retaining each point of η independently of each other with probability p ; see [46, Section 5.3]. A straightforward computation shows that the intensity γ_p and the reduced covariance measure $\beta_{2,p}^!$ of η_p are given by $\gamma_p = p\gamma$ and $\beta_{2,p}^! = p^2\beta_2^!$, respectively. Consequently, if the structure factor is defined via equation (2.9), we obtain

$$S_p(k) = 1 - p + pS(k), \quad k \in \mathbb{R}^d. \quad (8.1)$$

This identity holds for all k for which $S(k)$ (and hence $S_p(k)$) is well defined.

By thinning we gain fine control over the value of $s := S(0)$, the structure factor at the origin. We begin with $s = 10^{-4}$, which is an order of magnitude smaller than typical values encountered in non-hyperuniform models [59, 41], and increase s up to 0.1. For each combination of s and system size L , we generate 10 000 independent realizations of the point process.

Table 1 reports the fraction of samples for which the null hypothesis is rejected, rounded to two decimal places. These values provide an empirical measure of the power of the test. Crucially, recall that the test statistic T is evaluated separately for each

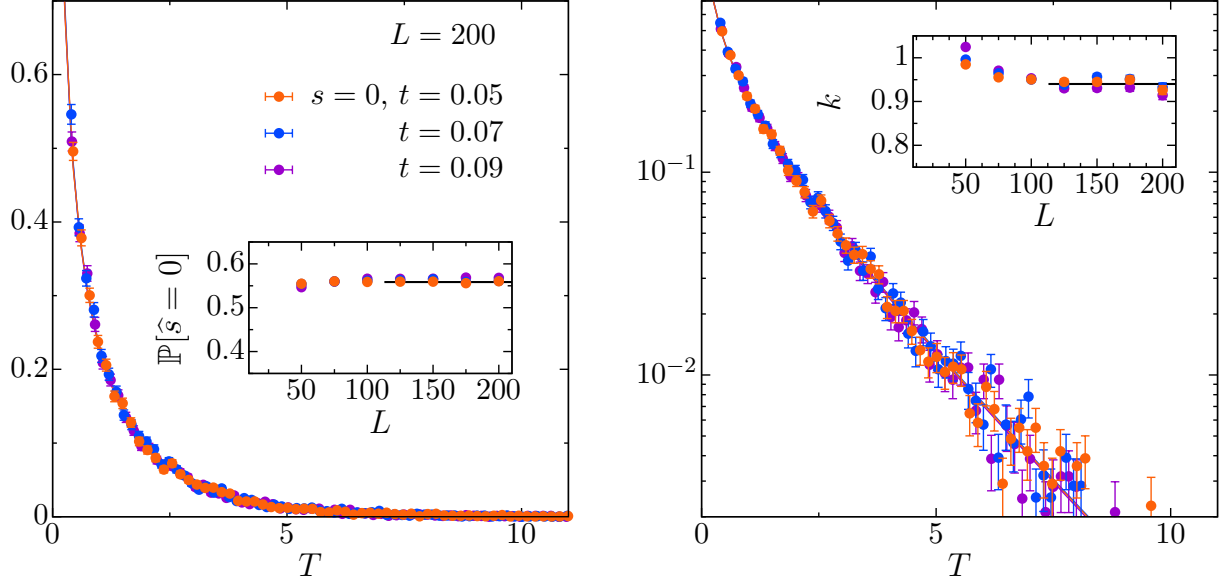


Figure 11: Density estimates for the continuous part of T (bullets) for matched point patterns, and densities of a χ^2 -distribution with the same expectation (solid lines). A linear plot is shown on the left-hand side, and a log-log plot on the right-hand side. The insets show the size of the atom of T (left) and the *fractional* parameter k of the χ^2 -distribution as a function of L . The solid lines in the inset indicate the universally chosen parameters for the test, i.e., an atom of size 0.5585 and a fractional parameter $k = 0.9400$.

realization, i.e., for single point patterns. An asterisk indicates that every sample in the corresponding setting leads to rejection, signifying power one. The nominal significance level is fixed at 0.05.

For all simulations, we set $\rho = 3.0$, corresponding to $t \approx 0.05$. The parameter $k_{<}$, determining the maximum wave vector length in equation (6.4), is set to 0.75, as before. We observed that modest increases in $k_{<}$ can enhance the power of the test while still preserving the significance level. However, if $k_{<}$ is chosen too large, the parabolic approximation underlying the test becomes invalid.

The first row of Table 1 confirms that the test maintains the nominal significance level under the null hypothesis, within statistical fluctuations. For any $s > 0$, the power increases rapidly with either the system size L or the magnitude of the structure factor s at the origin. Notably, even with relatively small samples containing just 2 500 points ($L = 50$), nearly all realizations are rejected when $s > 10^{-2}$. For the challenging case $s = 10^{-4}$, often regarded as a borderline scenario in physical applications [59, 41], the test still rejects over 90% of samples at $L = 300$, corresponding to 90 000 points.

9 Summary of test procedure

The novel test procedure is summarized below (for details, see the open-source implementation and its documentation [38]). As with any null hypothesis test, the first step is to specify a significance level, denoted ζ , e.g., 5%.

Next, one selects the hyperuniformity scaling exponent α and a taper function h ,

Table 1: Power of the novel test for hyperuniformity for a range of values of s and L . Each test is applied to only a single sample of the thinned model (v).

s	L						
	50	100	150	200	250	300	400
0.0	0.05	0.05	0.06	0.05	0.05	0.05	0.05
0.0001	0.08	0.20	0.41	0.63	0.82	0.93	0.99
0.00025	0.13	0.41	0.77	0.94	0.99	1.00	*
0.0005	0.20	0.69	0.96	1.00	*	*	*
0.00075	0.27	0.84	0.99	1.00	*	*	*
0.001	0.34	0.92	1.00	*	*	*	*
0.0025	0.67	1.00	*	*	*	*	*
0.005	0.88	*	*	*	*	*	*
0.0075	0.94	*	*	*	*	*	*
0.01	0.97	*	*	*	*	*	*
0.025	0.99	*	*	*	*	*	*
0.05	1.00	*	*	*	*	*	*
0.075	1.00	*	*	*	*	*	*
0.1	1.00	*	*	*	*	*	*

together with the corresponding wave vectors, based on the data, such as assumptions about the underlying model or measurement details. The default choice for α is two: values smaller than two require long-range correlations, whereas larger values demand a mechanism that suppresses the leading-order term. For simulated data with periodic boundary conditions, a standard choice of h is the cubic taper function described in Example 3.2, paired with the commensurable wave vectors K_L defined in (6.4).

The maximum wavenumber $k_<$ should be chosen at the onset of the so-called scaling regime of the scattering intensity, i.e., where the approximation (1.1) becomes valid. This value can be read directly from a log-log plot of $\mathcal{S}(k)$. The test is robust to the precise choice of this parameter; however, a value that is too small amplifies statistical fluctuations, while choosing it too large introduces systematic errors since approximation (1.1) is then violated.

Our implementation [38] proceeds as follows.

1. The critical value T_c of the test statistic is computed as

$$T_c := F_{\chi^2, k}^{-1} \left(\frac{1 - \zeta - \mathbb{P}_{s,t}(T = 0)}{1 - \mathbb{P}_{s,t}(T = 0)} \right),$$

where $F_{\chi^2, k}^{-1}$ denotes the inverse χ^2 -distribution with a fractional parameter $k = 0.9400$, and the atom of the distribution of T , $\mathbb{P}_{s,t}(T = 0) = 0.5585$, is taken into account. For a significance level of 5%, this yields $T_c \approx 2.382$.

2. In preparation of the actual test, the data are loaded, the parameters are read, and the wave vectors and corresponding scattering intensities are computed.

3. Under the null hypothesis, \hat{t}_0 is obtained from (6.3), and the corresponding h_0 is evaluated.
4. In the full parameter space, the log-likelihood $\mathcal{L}^*(\vartheta)$ from (6.6) is maximized, yielding \hat{s} , \hat{t}_1 , and h_1 as defined in (6.7), (6.9), and (6.10).
5. The test statistic $T = 2(h_1 - h_0)$ is evaluated.

The null hypothesis is accepted if $T < T_c$ and rejected otherwise.

10 Final remarks

Our test relies on three key approximations, each of which becomes valid in the same thermodynamic limit, that is, for large system sizes. First, in this limit, the scattering intensity becomes both exponentially distributed and independent across different wave vectors. Second, the number of available wave vectors in a neighborhood around the origin diverges, and the distribution of the test statistic converges to a specific mixture: a point mass at zero and a gamma distribution. Future work may establish that this convergence also holds for finite (but sufficiently large) sample sizes, provided the number of samples increases accordingly. Third, in the thermodynamic limit, the approximation (1.1) holds in the following sense: as the system size grows, wave vectors of smaller magnitude become accessible, thereby improving the approximation. Accordingly, the range of wave numbers used for fitting must be adjusted as the sample size increases.

An intriguing direction for future research is to expand the class of point processes that satisfy the core assumption (4.9); see Remark 5.1. Additional studies could also provide further insight into the asymptotic behavior of the maximum likelihood estimator and the test statistic, as suggested by the simulation results. To our knowledge, there are no existing results in the literature that directly address sequences of independent exponential random variables with varying means governed by constrained parameters.

We have applied the novel test in extensive simulations to thinnings of the matching process from [40]. Preliminary results for other point processes show similarly promising behavior. Finally, we will release an open-source Python package to support the application of our test to a wide variety of datasets. We greatly appreciate any feedback and suggestions.

11 Appendices

11.1 Proof of Proposition 3.4 (asymptotic covariances)

Proof. We first assume that $k \neq \mathbf{0}$ and $\ell \neq \mathbf{0}$. Without loss of generality, we can then assume that $k_r \ell_r \neq 0$ for all $r > 0$. Hence, we have

$$\begin{aligned} \mathbb{E}T_r(k_r)\overline{T_r(\ell_r)} &= \frac{1}{r^d}\mathbb{E}\left[\sum_{x,y\in\eta}h_r(x)h_r(y)e^{-i\langle k_r,x\rangle}e^{i\langle \ell_r,y\rangle}\right] \\ &= \frac{1}{r^d}\mathbb{E}\left[\sum_{x\in\eta}h_r(x)^2e^{-i\langle k_r,x\rangle}e^{i\langle \ell_r,x\rangle}\right] \\ &\quad + \frac{1}{r^d}\mathbb{E}\left[\sum_{x,y\in\eta}^{\neq}h_r(x)h_r(y)e^{-i\langle k_r,x\rangle}e^{i\langle \ell_r,y\rangle}\right]. \end{aligned}$$

By applying Campbell's formula (2.1) along with (2.2), this leads to

$$\begin{aligned} \mathbb{E}T_r(k_r)\overline{T_r(\ell_r)} &= \frac{\gamma}{r^d}\int h_r(x)^2e^{i\langle \ell_r-k_r,x\rangle}dx \\ &\quad + \frac{1}{r^d}\iint h_r(x)h_r(x+y)e^{-i\langle k_r,x\rangle}e^{i\langle \ell_r,x+y\rangle}dx\alpha_2^!(dy) \\ &=: C_1(r) + C_2(r), \end{aligned} \tag{11.1}$$

say. By (3.4), we obtain

$$\lim_{r\rightarrow\infty}C_1(r) = \gamma M_2(h)\mathbf{1}\{k = \ell\}.$$

From assumption (3.6), we also have

$$\lim_{r\rightarrow\infty}C_2(r) = \lim_{r\rightarrow\infty}C_2'(r),$$

where

$$C_2'(r) := \frac{1}{r^d}\iint h_r(x)h_r(x+y)e^{-i\langle k_r,x\rangle}e^{i\langle \ell_r,x+y\rangle}dx\beta_2^!(dy).$$

Rewriting $C_2'(r)$, we obtain

$$\begin{aligned} C_2'(r) &= \frac{1}{r^d}\iint h_r(x)h_r(x+y)e^{i\langle \ell_r-k_r,x\rangle}e^{i\langle \ell_r,y\rangle}dx\beta_2^!(dy) \\ &= \frac{1}{r^d}\iint h_r(x)^2e^{i\langle \ell_r-k_r,x\rangle}e^{i\langle \ell_r,y\rangle}dx\beta_2^!(dy) \\ &\quad + \frac{1}{r^d}\iint h_r(x)(h_r(x+y) - h_r(x))e^{i\langle \ell_r-k_r,x\rangle}e^{i\langle \ell_r,y\rangle}dx\beta_2^!(dy) \\ &=: D_1(r) + D_2(r), \end{aligned}$$

say. Furthermore,

$$D_1(r) = \frac{1}{r^d}\int h_r(x)^2e^{i\langle \ell_r-k_r,x\rangle}dx\int e^{i\langle \ell_r,y\rangle}\beta_2^!(dy).$$

If $(k_r) = (\ell_r)$, then

$$D_1(r) = M_2(h) \int e^{i\langle \ell_r, y \rangle} \beta_2^!(dy).$$

By assumption (3.1) and the dominated convergence theorem,

$$\lim_{r \rightarrow \infty} D_1(r) = M_2(h) \gamma(S(k) - 1).$$

From (3.4), in all other cases, we obtain $D_1(r) \rightarrow 0$ as $r \rightarrow \infty$.

We now show that $D_2(r) \rightarrow 0$ as $r \rightarrow \infty$. Let $c > 0$ be an upper bound for $|h|$. Then, using (3.3), we obtain

$$\begin{aligned} |D_2(r)| &\leq \frac{c}{r^d} \iint |h_r(x+y) - h_r(x)| dx |\beta_2^!|(dy) \\ &= c \iint |h(x+r^{-1}y) - h(x)| dx |\beta_2^!|(dy) \\ &\leq ca \int r^{-p} \|y\|^p |\beta_2^!|(dy) + 2M_1(h) \int \mathbf{1}\{\|y\| > rb\} |\beta_2^!|(dy). \end{aligned}$$

By (3.1) and (2.6), this upper bound tends to zero as $r \rightarrow \infty$.

It remains to consider the case where $k_r \equiv 0$. Since $\mathbb{E}T_r(0) = 0$ and the centring term of $T_r(0)$ (in the case $\ell_r \equiv 0$) is deterministic we then have

$$\begin{aligned} \mathbb{E}T_r(0) \overline{T_r(\ell_r)} &= \frac{1}{r^d} \mathbb{E} \left[\sum_{y \in \eta} h_r(y) \sum_{x \in \eta} h_r(x) e^{i\langle \ell_r, x \rangle} \right] - M_1(h) \gamma \mathbb{E} \left[\sum_{x \in \eta} h_r(x) e^{i\langle \ell_r, x \rangle} \right] \\ &= \frac{\gamma}{r^d} \int h_r(x)^2 e^{i\langle \ell_r, x \rangle} dx + \frac{1}{r^d} \iint h_r(x) h_r(x+y) e^{i\langle \ell_r, x \rangle} dx \alpha_2^!(dy) \\ &\quad - M_1(h) \gamma^2 \int h_r(x) e^{-i\langle \ell_r, x \rangle} dx. \end{aligned}$$

Since $\int h_r(x+y) dy = M_1(h) r^d$, $x \in \mathbb{R}^d$, we obtain

$$\begin{aligned} \mathbb{E}T_r(0) \overline{T_r(\ell_r)} &= \frac{\gamma}{r^d} \int h_r(x)^2 e^{i\langle \ell_r, x \rangle} dx \\ &\quad + \frac{1}{r^d} \iint e^{i\langle \ell_r, x \rangle} h_r(x) h_r(x+y) dx \beta_2^!(dy). \end{aligned} \tag{11.2}$$

If $\ell_r \equiv 0$, the first term equals $\gamma M_2(h)$. Otherwise, it tends to zero by (3.4). Similarly as before, we rewrite the second term as

$$\begin{aligned} &\frac{1}{r^d} \beta_2^!(\mathbb{R}^d) \int e^{i\langle \ell_r, x \rangle} h_r(x)^2 dx \\ &\quad + \frac{1}{r^d} \iint e^{-i\langle \ell_r, x \rangle} h_r(x) (h_r(x+y) - h_r(x)) dx \beta_2^!(dy). \end{aligned} \tag{11.3}$$

Here, the second term tends to 0 as $r \rightarrow \infty$, and so does the first term if $(\ell_r) \neq \mathbf{0}$. If $(\ell_r) = \mathbf{0}$ the first term equals $M_2(h) \beta_2^!(\mathbb{R}^d) = M_2(h) \gamma(S(0) - 1)$. \square

11.2 Proof of Theorem 4.1 (central limit theorem)

We adapt the classical methods from [10] to our spatial setting. For a finite non-empty set M , let Π_M denote the set of all partitions of M . For $n \in \mathbb{N}$ we abbreviate $\Pi_n := \Pi_{[n]}$. Let $m \in \mathbb{N}$, and let X_1, \dots, X_m be complex-valued random variables satisfying $\mathbb{E}|X_j|^m < \infty$ for each $j \in [m]$. The (joint) *cumulant* of these random variables is defined as

$$\text{Cum}(X_1, \dots, X_m) = \sum_{\sigma \in \Pi_m} (-1)^{|\sigma|-1} (|\sigma| - 1)! \prod_{I \in \sigma} \mathbb{E} \prod_{i \in I} X_i. \quad (11.4)$$

For real-valued random variables, (11.4) is not the definition but rather a fundamental property; see, e.g., [55, Proposition 3.2.1]. However, following [10], we use (11.4) as a natural multilinear extension of the cumulant to random vectors with complex-valued components. The inverse relation of (11.4) is given by

$$\mathbb{E} X_1 \cdots X_m = \sum_{\sigma \in \Pi_m} \prod_{I \in \sigma} \text{Cum}((X_j)_{j \in I}). \quad (11.5)$$

For any measurable function $f: \mathbb{R}^d \rightarrow \mathbb{C}$, we define

$$\eta(f) := \sum_{x \in \eta} f(x).$$

Let $m \in \mathbb{N}$, and let $f_1, \dots, f_m: \mathbb{R}^d \rightarrow \mathbb{C}$ be measurable and bounded functions. For $I \subset [m]$, we define $f_I: \mathbb{R}^d \rightarrow \mathbb{C}$ by $f_I(x) := \prod_{i \in I} f_i(x)$, $x \in \mathbb{R}^d$. Using (11.4) and following the argument presented in the proof of [30, Lemma 1], one can show that

$$\text{Cum}(\eta(f_1), \dots, \eta(f_m)) = \sum_{i=1}^m \sum_{\sigma \in \Pi_{m,i}} \int \prod_{j=1}^i f_{I_j(\sigma)}(x_j) \beta_i(d(x_1, \dots, x_i)), \quad (11.6)$$

where we write $\sigma = \{I_1(\sigma), \dots, I_i(\sigma)\}$ for $\sigma \in \Pi_{m,i}$ and assume that

$$\int \prod_{j=1}^i |f_{I_j(\sigma)}(x_j)| |\beta_i|(d(x_1, \dots, x_i)) < \infty, \quad \sigma \in \Pi_{m,i}, i \leq m. \quad (11.7)$$

For the benefit of the reader, and since the argument applies to point processes on a general state space, we outline the key idea behind the proof of (11.6). We first assume that f_1, \dots, f_m vanish outside a bounded set. It is not difficult to see (see [15, Exercise 5.4.5]) that, under this condition,

$$\mathbb{E} \prod_{i \in I} \eta(f_i) = \sum_{\pi \in \Pi_I} \int \prod_{J \in \pi} f_J(x_J) \alpha_{|\pi|}(d(x_J)_{J \in \pi}).$$

Substituting this expression into (11.4) yields

$$\begin{aligned} \text{Cum}(\eta(f_1), \dots, \eta(f_m)) &= \sum_{\sigma \in \Pi_m} (-1)^{|\sigma|-1} (|\sigma| - 1)! \\ &\quad \times \prod_{I \in \sigma} \sum_{\pi \in \Pi_I} \int \prod_{J \in \pi} f_J(x_J) \alpha_{|\pi|}(d(x_J)_{J \in \pi}). \end{aligned}$$

We now express the product over $I \in \sigma$ as a sum over $\pi_1 \in \Pi_{I_1(\sigma)}, \dots, \pi_{|\sigma|} \in \Pi_{I_{|\sigma|}(\sigma)}$ and then swap the summation with that over σ . This reordering results in a sum over $\pi \in \Pi_m$, followed by a sum over $\sigma \in \Pi_\pi$. Finally, using definition (4.4) with π instead of $[m]$, we obtain (11.6).

If some of the f_1, \dots, f_m do not have a bounded support, we can apply (11.6) to their restrictions f_1^r, \dots, f_m^r to the ball B_r , $r > 0$. By assumption (11.7) and dominated convergence, the corresponding right-hand side of (11.6) converges, as $r \rightarrow \infty$, to the right-hand side of (11.6). This remains true if we replace the functions f_1, \dots, f_m by their absolute values. But then we can use (11.5) and monotone convergence too see that $\mathbb{E}\eta(|f_j|)^m < \infty$ for each $j \in [m]$. Finally it follows from definition (11.4) and dominated convergence that

$$\lim_{r \rightarrow \infty} \text{Cum}(\eta(f_1^r), \dots, \eta(f_m^r)) = \text{Cum}(\eta(f_1), \dots, \eta(f_m)),$$

concluding the proof of (11.6) in the general case.

We now consider $m \geq 3$, $r > 0$, and $k_1(r), \dots, k_m(r) \in \mathbb{R}^d$. Since the dependence of $k_i(r)$ on r is not essential in the following discussion, we omit it from our notation. (In view of (4.3), this constitutes a slight abuse of notation.) Applying equation (11.6) with the functions $f_j := h_r e^{-i\langle k_j, \cdot \rangle}$, $j \in [m]$, the right-hand side of (11.6), denoted by $A(r)$, simplifies to

$$A(r) = \sum_{i=1}^m \sum_{\sigma \in \Pi_{m,i}} \int \prod_{q=1}^i \prod_{j \in I_q(\sigma)} h_r(x_q) e^{-i\langle k_j, x_q \rangle} \beta_i(d(x_1, \dots, x_i)).$$

Replacing the integrands by their absolute values and the measures β_i by $|\beta_i|$, we can use the integrability of h and the identity

$$|\beta_m|(\cdot) = \iint \mathbf{1}\{(x, x_1 + x, \dots, x_{m-1} + x) \in \cdot\} |\beta_m^!|(d(x_1, \dots, x_{m-1})) dx$$

to confirm assumption (11.7). Defining $k' := k_1 + \dots + k_m$ and using (4.7), we obtain

$$\begin{aligned} A(r) &= \sum_{i=1}^m \sum_{\sigma \in \Pi_{m,i}} \iint \prod_{j \in I_1(\sigma)} h_r(x) e^{-i\langle k_j, x \rangle} \\ &\quad \times \prod_{q=2}^i \prod_{j \in I_q(\sigma)} h_r(x + x_q) e^{-i\langle k_j, x_q \rangle} e^{-i\langle k_j, x \rangle} \beta_i^!(d(x_2, \dots, x_i)) dx \\ &= \sum_{i=1}^m \sum_{\sigma \in \Pi_{m,i}} \iint e^{-i\langle k', x \rangle} h_r(x)^{|I_1(\sigma)|} \\ &\quad \times \prod_{q=2}^i \prod_{j \in I_q(\sigma)} h_r(x + x_q) e^{-i\langle k_j, x_q \rangle} \beta_i^!(d(x_2, \dots, x_i)) dx, \end{aligned}$$

where the term for $i = 1$ should be interpreted appropriately. Now, suppose $a_1, b_1, \dots, a_m, b_m \in \mathbb{R}$ are bounded in absolute value by some constant $c > 1$. It then follows by induction

(using the identity $ab - cd = (a - c)b + (b - d)c$)

$$\left| \prod_{j=1}^m a_j - \prod_{j=1}^m b_j \right| \leq c^{m-1} \sum_{j=1}^m |a_j - b_j|.$$

Letting c be an upper bound of $|h|$, and defining $c_1 := mc^{m-1}$, we obtain, for each $\sigma \in \Pi_{m,i}$, that

$$\begin{aligned} & \left| h_r(x)^{|I_1(\sigma)|} \prod_{j=2}^i h_r(x_j + x)^{|I_j(\sigma)|} - h_r(x)^m \right| \\ & \leq mc^{m-1} \sum_{j=2}^i |I_j(\sigma)| |h_r(x_j + x) - h_r(x)| \\ & \leq c_1 \sum_{j=2}^i |h_r(x_j + x) - h_r(x)|. \end{aligned}$$

It follows that $A(r) = A_1(r) + A_2(r)$, where

$$\begin{aligned} A_1(r) &:= \sum_{i=1}^m \sum_{\sigma \in \Pi_{m,i}} \iint e^{-i\langle k', x \rangle} h_r(x)^m \\ & \quad \times \prod_{j=2}^i \prod_{i \in I_j(\sigma)} e^{-i\langle k_i, x_j \rangle} \beta_n^!(d(x_2, \dots, x_i)) dx, \end{aligned}$$

and $A_2(r)$ satisfies

$$\begin{aligned} |A_2(r)| &\leq c_2 \sum_{i=2}^m \sum_{j=2}^i \iint |h_r(x_j + x) - h_r(x)| dx |\beta_i^!|(d(x_2, \dots, x_i)) \\ &= c_2 r^d \sum_{i=2}^m \sum_{j=2}^i \iint |h(r^{-1}x_j + x) - h(x)| dx |\beta_i^!|(d(x_2, \dots, x_i)) \end{aligned} \quad (11.8)$$

for some $c_2 > 0$. By assumption (4.8) and the fact that $\int h(x)^m dx < \infty$, we conclude that

$$|A_1(r)| \leq c_3 r^d, \quad r > 0, \quad (11.9)$$

for some constant $c_3 > 0$. Additionally, since $\int |h(z + x) - h(x)| dx \leq 2M_1(h)$ for all $z \in \mathbb{R}^d$, the same bound applies to $|A_2(r)|$. If $k_j \neq 0$ then $T_r(k_j) = r^{-d/2} \eta(f_j)$. Since the cumulant is homogeneous in each variable, it follows that

$$\lim_{r \rightarrow \infty} \text{Cum}(T_r(k_1(r)), \dots, T_r(k_m(r))) = 0, \quad m \geq 3. \quad (11.10)$$

This remains true if one of the k_j equals 0, because the cumulant is translation invariant.

Recall that $T_{r,1}(k)$ denotes the real part and $T_{r,2}(k)$ the imaginary part of $T_r(k)$. Let us abbreviate $(X'_j, Y'_j, Z'_j) := (T_{r,1}(k_j), T_{r,2}(k_j), T_r(k_j))$. By the multilinearity of cumulants,

$\text{Cum}(X'_1, Z'_2, \dots, Z'_m)$ and $\text{Cum}(Y'_1, Z'_2, \dots, Z'_m)$ are linear functions of $\text{Cum}(Z'_1, \dots, Z'_m)$ and $\text{Cum}(\overline{Z}'_1, Z_2, \dots, Z_m)$. Let $W_j \in \{X'_j, Y'_j\}$ for $j \in [m]$. By induction, it follows that $\text{Cum}(W_1, \dots, W_m)$ is a linear function of cumulants $\text{Cum}(V_1, \dots, V_m)$, where $V_j \in \{Z'_j, \overline{Z}'_j\}$. Since we may apply (11.10) with k'_j in place of k_j , where $k'_j \in \{k_1, -k_1, \dots, k_m, -k_m\}$, and because $T_r(-k_j) = \overline{T}_r(k_j)$, we obtain

$$\lim_{r \rightarrow \infty} \text{Cum}(Z_r(k_1(r)), \dots, Z_r(k_m(r))) = 0, \quad k_1, \dots, k_m \in \mathbb{R}^d, \quad m \geq 3, \quad (11.11)$$

where $Z_r(k_j) \in \{T_{r,1}(k_\ell), T_{r,2}(k_\ell) : \ell \in [m]\}$ for each $j \in [m]$.

With these preliminaries in place, we now turn to the proof of the convergence (4.3). Let $a_1, b_1, \dots, a_n, b_n$ be real numbers. By the Cramér–Wold device, it suffices to show that

$$Z_r := \sum_{j=1}^n (a_j T_{r,1}(k_{j,r}) + b_j T_{r,2}(k_{j,r})) \xrightarrow{d} \sum_{j=1}^n (a_j X_j + b_j Y_j), \quad \text{as } r \rightarrow \infty,$$

where $X_1, Y_1, \dots, X_n, Y_n$ are independent, normally distributed random variables with mean 0 and variances $\gamma M_2(h)S(k_1)/2, \dots, \gamma M_2(h)S(k_n)/2$, respectively. To prove this, we use the method of moments (see, e.g., [4, Section 30], or [31, Section 3]). By equations (11.4) and (11.5), cumulants and moments are in a one-to-one (polynomial) correspondence, so convergence in distribution can be established by showing the convergence of the cumulants. Specifically, for $m \in \mathbb{N}$, the m -th cumulant of Z_r is defined by $C_m(Z_r) := \text{Cum}(Z_r, \dots, Z_r)$, where Z_r appears m times. From (11.11) and multilinearity, it follows that

$$\lim_{r \rightarrow \infty} C_m(Z_r) = 0, \quad m \geq 3.$$

From (3.17) and (3.11), we further conclude that

$$\lim_{r \rightarrow \infty} \text{Var}(Z_r) = \frac{\gamma}{2} \sum_{j=1}^n (a_j^2 + b_j^2) M_2(h)S(k_j),$$

which matches the variance of $\sum_{j=1}^n (a_j X_j + b_j Y_j)$. It only remains to invoke once again (3.11) to ensure convergence of the first moments.

Remark 11.1. It is worth noting that the proof of the convergence (11.10) requires only that h be bounded and integrable, along with the hypothesis (4.8) regarding the reduced cumulant measures of order $m \geq 3$. The conditions (3.6) and (3.3) are not needed. Hence, the CLT (4.3) remains valid in a more general setting, provided that the asymptotic expectations (3.11) and covariances (3.15) exist as finite limits.

11.3 Properties of the likelihood function

Here we discuss some properties of the likelihood function \mathcal{L}^* defined by (6.5). Using (6.6) and some straightforward calculations, we obtain

$$\begin{aligned} \mathcal{L}^*(\vartheta) &= - \sum_{j=1}^n \log(\cos \vartheta + \kappa_j \sin \vartheta) - n \log \left(\sum_{j=1}^n \frac{x_j}{\cos \vartheta + \kappa_j \sin \vartheta} \right) \\ &\quad + n(\log n - 1). \end{aligned} \quad (11.12)$$

The derivative of \mathcal{L}^* is given by

$$\frac{d}{d\vartheta} \mathcal{L}^*(\vartheta) = \sum_{j=1}^n \frac{\sin \vartheta - \kappa_j \cos \vartheta}{\cos \vartheta + \kappa_j \sin \vartheta} + n \cdot \frac{\sum_{j=1}^n \frac{x_j(-\sin \vartheta + \kappa_j \cos \vartheta)}{(\cos \vartheta + \kappa_j \sin \vartheta)^2}}{\sum_{j=1}^n \frac{x_j}{\cos \vartheta + \kappa_j \sin \vartheta}}. \quad (11.13)$$

Regarding the limits of $\mathcal{L}^*(\vartheta)$ as $\vartheta \uparrow \pi/2$ and $\vartheta \downarrow \vartheta_0$, we have the following result:

Lemma 11.2. a) $\lim_{\vartheta \uparrow \pi/2} \mathcal{L}^*(\vartheta) = -\sum_{j=1}^n \log \kappa_j - n \log \left(\sum_{j=1}^n \frac{x_j}{\kappa_j} \right) + n(\log n - 1),$

b) If $\kappa_1 = \dots = \kappa_n$, then $\lim_{\vartheta \downarrow \vartheta_0} \mathcal{L}^*(\vartheta) = -n \log \left(\sum_{j=1}^n x_j \right) + n(\log n - 1),$

c) If at least two of the κ_j differ from each other, then $\lim_{\vartheta \downarrow \vartheta_0} \mathcal{L}^*(\vartheta) = -\infty.$

Proof. Part a) follows readily from (11.12), since $\cos \frac{\pi}{2} = 0$ and $\sin \frac{\pi}{2} = 1$. To prove b), let $\kappa := \kappa_1 = \dots = \kappa_n$. Using $\log \frac{a}{b} = \log a - \log b$, we obtain

$$\begin{aligned} \mathcal{L}^*(\vartheta) &= n \log(\cos \vartheta + \kappa \sin \vartheta) - n \log \left(\sum_{j=1}^n \frac{x_j}{\cos \vartheta + \kappa \sin \vartheta} \right) + n(\log n - 1) \\ &= -n \log \left(\sum_{j=1}^n x_j \right) + n \log n - 1, \end{aligned}$$

proving the assertion. To show c), assume without loss of generality that the κ_j are ordered so that $\kappa_1 \leq \dots \leq \kappa_n$. Moreover, suppose $\kappa_1 \leq \dots \leq \kappa_\ell < \kappa_{\ell+1} = \dots = \kappa_n$ for some $\ell \in \{1, \dots, n-1\}$. Setting $t := 1 + \kappa_n \tan \vartheta$, the limit $\vartheta \downarrow \vartheta_0$ corresponds to $t \downarrow 0$. Starting from (11.12) and using the definitions of ℓ and t , we obtain

$$\begin{aligned} \mathcal{L}^*(\vartheta) &= -\sum_{j=1}^{\ell} \log(\cos \vartheta + \kappa_j \sin \vartheta) - (n - \ell) \log(t \cos \vartheta) \\ &\quad - n \log \left(\frac{1}{t} \left\{ t \sum_{j=1}^{\ell} \frac{x_j}{\cos \vartheta + \kappa_j \sin \vartheta} + \frac{1}{\cos \vartheta} \sum_{j=\ell+1}^n x_j \right\} \right) + n(\log n - 1). \end{aligned}$$

Writing $O(1)$ for a term that is bounded as $t \downarrow 0$, and using the identity $\log(ab) = \log a + \log b$, it follows that

$$\mathcal{L}^*(\vartheta) = \ell \log t + O(1) \quad \text{as } t \downarrow 0.$$

Since $\ell \geq 1$, the proof is completed. \square

Although we do not have further mathematical results on the behavior of the function \mathcal{L}^* , there is strong heuristic evidence that \mathcal{L}^* has a unique maximizer $\widehat{\vartheta} \in (\vartheta_0, \pi/2]$, at least for the classes of problems that arise in typical applications. Moreover, this maximizer is equal to $\pi/2$ if the left-hand derivative of \mathcal{L}^* at $\pi/2$ is positive, and negative if this left-hand derivative is negative. From (11.13), it follows that

$$(\mathcal{L}^*)' \left(\frac{\pi}{2} - \right) := \lim_{\vartheta \uparrow \pi/2} \frac{d}{d\vartheta} \mathcal{L}^*(\vartheta) = \sum_{j=1}^n \frac{1}{\kappa_j} - n \cdot \frac{\sum_{j=1}^n \frac{x_j}{\kappa_j^2}}{\sum_{j=1}^n \frac{x_j}{\kappa_j}},$$

which implies

$$(\mathcal{L}^*)' \left(\frac{\pi}{2} - \right) > 0 \iff \sum_{j=1}^n \frac{x_j}{\kappa_j} \left(\frac{1}{n} \sum_{i=1}^n \frac{1}{\kappa_i} - \frac{1}{\kappa_j} \right) > 0.$$

Acknowledgments

We thank two anonymous referees, the authors of [26], Philipp Neumann, D. Yogeshwaran and Joe Yukich for many helpful comments. This research was supported by the Initiative and Networking Fund of the Helmholtz Association through the Project ‘DataMat’, as well as by the Deutsche Forschungsgemeinschaft (DFG, German Research Foundation) as part of the DFG priority program ‘Random Geometric Systems’ SPP 2265) under grants KL 3391/2-2, LA 965/11-1/2, LO 418/25-1, ME 1361/16-1, and WI 5527/1-1, and by the Volkswagenstiftung via the ‘Experiment’ Project ‘Finite Projective Geometry’.

References

- [1] ATKINSON, S., ZHANG, G., HOPKINS, A. B., AND TORQUATO, S. (2016). Critical slowing down and hyperuniformity on approach to jamming. *Phys. Rev. E* **94**, 012902-1–14.
- [2] BACKOFEN, R., ALTAWIL, A.Y.A., SALVALAGLIO, M., AND VOIGT, A. (2024). Nonequilibrium hyperuniform states in active turbulence. *PNAS* **121**, e2320719121.
- [3] BERG, C. AND FORST, G. (1975). *Potential Theory on Locally Compact Abelian Groups*. Springer, New-York.
- [4] BILLINGSLEY, P. (1995). *Probability and Measure*. Third Edition, Wiley, New York.
- [5] BISCIO, C.A. AND LAVANCIER, F. (2016). Brillinger mixing of determinantal point processes and statistical applications. *Electron. J. Stat.* **10**, 582–607.
- [6] BISCIO, C.A.N. AND WAAGEPETERSEN, R. (2019). A general central limit theorem and a subsampling variance estimator for α -mixing point processes. *Scand. J. Stat.* **46**, 1168–1190.

- [7] BJÖRKLUND, M. AND HARTNICK, T. (2024). Hyperuniformity and non-hyperuniformity of quasicrystals. *Math. Ann.* **389**, 365–426.
- [8] BŁASZCZYSZYN, B., YOGESHWARAN D., AND YUKICH, J.E. (2019). Limit theory for geometric statistics of point processes having fast decay of correlations. *Ann. Probab.* **47**, 835–895.
- [9] BRÉMAUD, P. (2020). *Point Process Calculus in Time and Space*. Springer, Cham.
- [10] BRILLINGER, D.R. (2012). The spectral analysis of stationary interval functions. In: *Selected Works of David Brillinger* (pp. 25-55). Springer, New York.
- [11] CAMILIER, I. AND DECREUSEFOND, L. (2010). Quasi-invariance and integration by parts for determinantal and permanental processes. *J. Funct. Anal.* **259**, 268–300.
- [12] CHATTERJEE, S. (2019). Rigidity of the three-dimensional hierarchical Coulomb gas. *Probab. Theory Related Fields* **175**, 1123–1176.
- [13] CHEN, D., ZHENG, Y., LIU, L., ZHANG, G., CHEN, M., JIAO, Y., AND ZHUANG, H. (2021). Stone–Wales defects preserve hyperuniformity in amorphous two-dimensional networks. *Proc. Natl. Acad. Sci. U.S.A.* **118**, e2016862118–1–9.
- [14] CHIU, S.N., STOYAN, D., KENDALL, W.S., AND MECKE, J. (2013). *Stochastic Geometry and its Applications*. Third Edition. Wiley, Chichester.
- [15] DALEY, D.J. AND VERE-JONES, D. (2003/2008). *An Introduction to the Theory of Point Processes. Volume I: Elementary Theory and Methods, Volume II: General Theory and Structure*. Second Edition. Springer, New York.
- [16] DEREUDRE, D., FLIMMEL, D., HUESMANN, M., AND LEBLÉ, T. (2024). (Non)-hyperuniformity of perturbed lattices. arXiv:2405.19881.
- [17] DREYFUS, R., XU, Y., STILL, T., HOUGH, L. A., YODH, A. G., AND TORQUATO, S. (2015). Diagnosing hyperuniformity in two-dimensional, disordered, jammed packings of soft spheres. *Phys. Rev. E* **91**, 012302.
- [18] GABRIELLI, A. (2004). Point Processes and Stochastic Displacement Fields. *Phys. Rev. E* **70**, 066131-1–16.
- [19] GABRIELLI, A., JANCOVICI, B., JOYCE, M., LEBOWITZ, J. L., PIETRONERO, L., AND LABINI, F.S. (2003). Generation of primordial cosmological perturbations from statistical mechanical models. *Phys. Rev. D*, **67**, 043506.
- [20] GALLIANO, L., CATES, M.E., AND BERTHIER, L. (2023). Two-dimensional crystals far from equilibrium. *Phys. Rev. Lett.* **131**, 047101.
- [21] GHOSH, S. AND LEBOWITZ, J. L. (2017). Fluctuations, large deviations and rigidity in hyperuniform systems: A brief survey. *Indian J. Pure Appl. Math.* **48**, 609–631.
- [22] GHOSH, S. AND LEBOWITZ, J. L. (2017). Number rigidity in superhomogeneous random point fields. *J. Stat. Phys.* **166**, 1016–1027.

- [23] GORSKY, S., BRITTON, W. A., CHEN, Y., MONTANER, J., LENEFF, A., RAUKAS, M., AND DAL NEGRO, L. (2019). Engineered hyperuniformity for directional light extraction. *APL Photonics* **4**, 110801.
- [24] GRAFAKOS, L. (2009). *Modern Fourier Analysis*. Second Edition, vol. 250, Springer, New York.
- [25] HANSEN, J.-P. AND McDONALD, I. R. (2013). *Theory of Simple Liquids: With Applications to Soft Matter*. Fourth Edition, Academic Press, Amsterdam. 2013.
- [26] HAWAT, D., GAUTIER, G., BARDENET, R., AND LACHIÈZE-REY, R. (2023). On estimating the structure factor of a point process, with applications to hyperuniformity. *Stat Comput* **33**, 61–1–28.
- [27] HEINRICH, L. (2016). On the strong Brillinger-mixing property of α -determinantal point processes and some applications. *Appl. Math.* **61**, 443–461.
- [28] HEINRICH, L. AND KLEIN, S. (2014). Central limit theorems for empirical product densities of stationary point processes. *Stat. Inference Stoch. Process.* **17**, 121–138.
- [29] HEINRICH, L. AND PROKEŠOVÁ, M. (2010). On estimating the asymptotic variance of stationary point processes. *Methodol. Comput. Appl. Probab.* **12**, 451–471.
- [30] HEINRICH, L. AND SCHMIDT, V. (1985). Normal convergence of multidimensional shot noise and rates of this convergence. *Adv. Appl. Probab.* **17**, 709–730.
- [31] HENZE, N. (2024). *Asymptotic Stochastics. An Introduction with a View towards Statistics*. Mathematics Study Resources Vol. 10. Springer Nature, Berlin.
- [32] HOUGH, J.B., KRISHNAPUR, M., PERES, Y., AND VIRAG, B. (2010). *Zeros of Gaussian Analytic Functions and Determinantal Point Processes*. A.M.S., 2010.
- [33] HUANG, M., HU, W., YANG, S., LIU, Q.-X., AND ZHANG, H. P. (2021). Circular swimming motility and disordered hyperuniform state in an algae system. *Proc. Natl. Acad. Sci. U.S.A.* **118**, e2100493118–1–8.
- [34] HUESMANN M., AND LEBLÉ, T. (2026). The link between hyperuniformity, Coulomb energy and Wasserstein distance to Lebesgue for two-dimensional point processes. *Probab. Math. Phys.* **7**, 123–173.
- [35] JIAO, Y., LAU, T., HATZIKIROU, H., MEYER-HERMANN, M., CORBO, J. C., AND TORQUATO, S. (2014). Avian photoreceptor patterns represent a disordered hyperuniform solution to a multiscale packing problem. *Phys. Rev. E* **89**, 022721.
- [36] KALLENBERG, O. (2002). *Foundations of Modern Probability*. Second Edition, Springer, New York.
- [37] KIM, J. AND TORQUATO, S. (2018). Effect of imperfections on the hyperuniformity of many-body systems. *Phys. Rev. B* **97**, 054105.

- [38] KLATT, M. A. (2025+). Open source implementation, to be published with the paper.
- [39] KLATT, M. A., KIM, J., AND TORQUATO, S. (2020). Cloaking the underlying long-range order of randomly perturbed lattices. *Phys. Rev. E* **101**, 032118.
- [40] KLATT, M., LAST, G., AND YOGESHWARAN, D. (2020). Hyperuniform and rigid stable matchings. *Random Struct. Algor.* **57**, 439–473.
- [41] KLATT, M. A., LOVRIĆ, J., CHEN, D., KAPFER, S. C., SCHALLER, F. M., SCHÖNHÖFER, P. W., A., GARDINER, B. S., SMITH, A.-S., SCHRÖDER-TURK, G. E., AND TORQUATO, S. (2019). Universal hidden order in amorphous cellular geometries. *Nat. Commun.* **10**, 811.
- [42] KLATT, M. A., LAST, G., LOTZ, L., YOGESHWARAN, D. (2025). Invariant transports of stationary random measures: asymptotic variance, hyperuniformity, and examples. arXiv:2506.05907.
- [43] KLATT, M. A. AND TORQUATO, S. (2016). Characterization of maximally random jammed sphere packings. II. Correlation functions and density fluctuations. *Phys. Rev. E* **94**, 022152.
- [44] LACHIÈZE-REY, R. (2022). Diophantine Gaussian excursions and random walks. *Electron. J. Probab.* **27**, 126-1–33.
- [45] LACHIÈZE-REY, R. AND YOGESHWARAN, D. (2024). Hyperuniformity and optimal transport of point processes. arXiv:2402.13705
- [46] LAST, G. AND PENROSE, M. (2017). *Lectures on the Poisson Process*. Cambridge University Press.
- [47] LAVANCIER, F., MØLLER, J., AND RUBAK, E. (2015). Determinantal point process models and statistical inference. *J. R. Stat. Soc., Ser. B, Stat. Methodol.*, **77**, 853–877.
- [48] LEI, Q.-L., CIAMARRA, M. P., AND NI, R. (2019). Nonequilibrium strongly hyperuniform fluids of circle active particles with large local density fluctuations. *Sci. Adv.* **5**, eaau7423.
- [49] LIU, Y., LI, X., TIAN, J., YAN, X., AND ZHANG, G. (2025). Impact of random spatial truncation and reciprocal-space binning on the detection of hyperuniformity in disordered systems. arXiv:2511.15009
- [50] MASTRILLI, G. (2025) Asymptotic fluctuations of smooth linear statistics of independently perturbed lattices. arXiv:2503.02627
- [51] MASTRILLI, G., BŁASZCZYŚZYN, B., AND LAVANCIER F. (2025). Estimating the hyperuniformity exponent of point processes. arXiv:2407.16797
- [52] MUGGLESTONE, M. A. AND RENSHAW, E. (1996). A practical guide to the spectral analysis of spatial point processes. *Comput. Statist. Data Anal.*, **21**, 43–65.

- [53] NAZAROV, F. AND SODIN, M. (2012). Correlation functions for random complex zeroes: strong clustering and local universality. *Commun. Math. Phys.* **310**, 75–98.
- [54] NIZAM Ü., S., MAKEY, G., BARBIER, M., KAHRAMAN, S. S., DEMIR, E., SHAFIGH, E. E., GALIOGLU, S., VAHABLI, D., HÜSNÜGİL, S., GÜNEŞ, M. H., YELESTI, E., AND ILDAY, S. (2021). Dynamic evolution of hyperuniformity in a driven dissipative colloidal system. *J. Phys.: Condens. Matter* **33**, 304002–1–28.
- [55] PECCATI, G. AND TAQQU, M. S. (2011). *Wiener Chaos: Moments, Cumulants and Diagrams: A survey with computer implementation*. Springer, Milan.
- [56] RAJALA, T. A., OLHEDE, S. C., GRAINGER, J. P., AND MURRELL, D. J. (2023). What is the Fourier transform of a spatial point process? *IEEE Trans. Inform. Theory* **69**, 5219–5252.
- [57] SHIRAI, T. AND TAKAHASHI, Y. (2003). Random point fields associated with certain Fredholm determinants I: fermion, Poisson and boson point processes. *J. Funct. Anal.* **205**, 414–463.
- [58] SKOLNICK, M. AND TORQUATO, S. (2023). Simulated diffusion spreadability for characterizing the structure and transport properties of two-phase materials, *Acta Mater.* **250**, 118857.
- [59] TORQUATO, S. (2018). Hyperuniform states of matter. *Phys. Rep.* **745**, 1–95.
- [60] TORQUATO, S., KIM, J., AND KLATT, M. A. (2021). Local Number Fluctuations in Hyperuniform and Nonhyperuniform Systems: Higher-Order Moments and Distribution Functions. *Phys. Rev. X* **11**, 021028–1–27.
- [61] TORQUATO, S. AND STILLINGER, F.H. (2003). Local density fluctuations, hyperuniformity, and order metrics *Phys. Rev. E* **68**, 041113.
- [62] UCHE, O. U., TORQUATO, S., AND STILLINGER, F. H. (2006). Collective coordinate control of density distributions. *Phys. Rev. E* **74**, 046122-1–9.
- [63] WILKEN, S., GUERRA, R. E., LEVINE, D., AND CHAIKIN, P. M. (2021). Random Close Packing as a Dynamical Phase Transition. *Phys. Rev. Lett.* **127**, 038002–1–6.
- [64] ZHANG, G. AND TORQUATO, S. (2013). Precise algorithm to generate random sequential addition of hard hyperspheres at saturation. *Phys. Rev. E* **88**, 053312–1–9.
- [65] ZHENG, Y., LIU, L., NAN, H., SHEN, Z.-X., ZHANG, G., CHEN, D., HE, L., XU, W., CHEN, M., JIAO, Y., AND ZHUANG, H. (2020). Disordered hyperuniformity in two-dimensional amorphous silica. *Sci. Adv.* **6**, eaba0826.